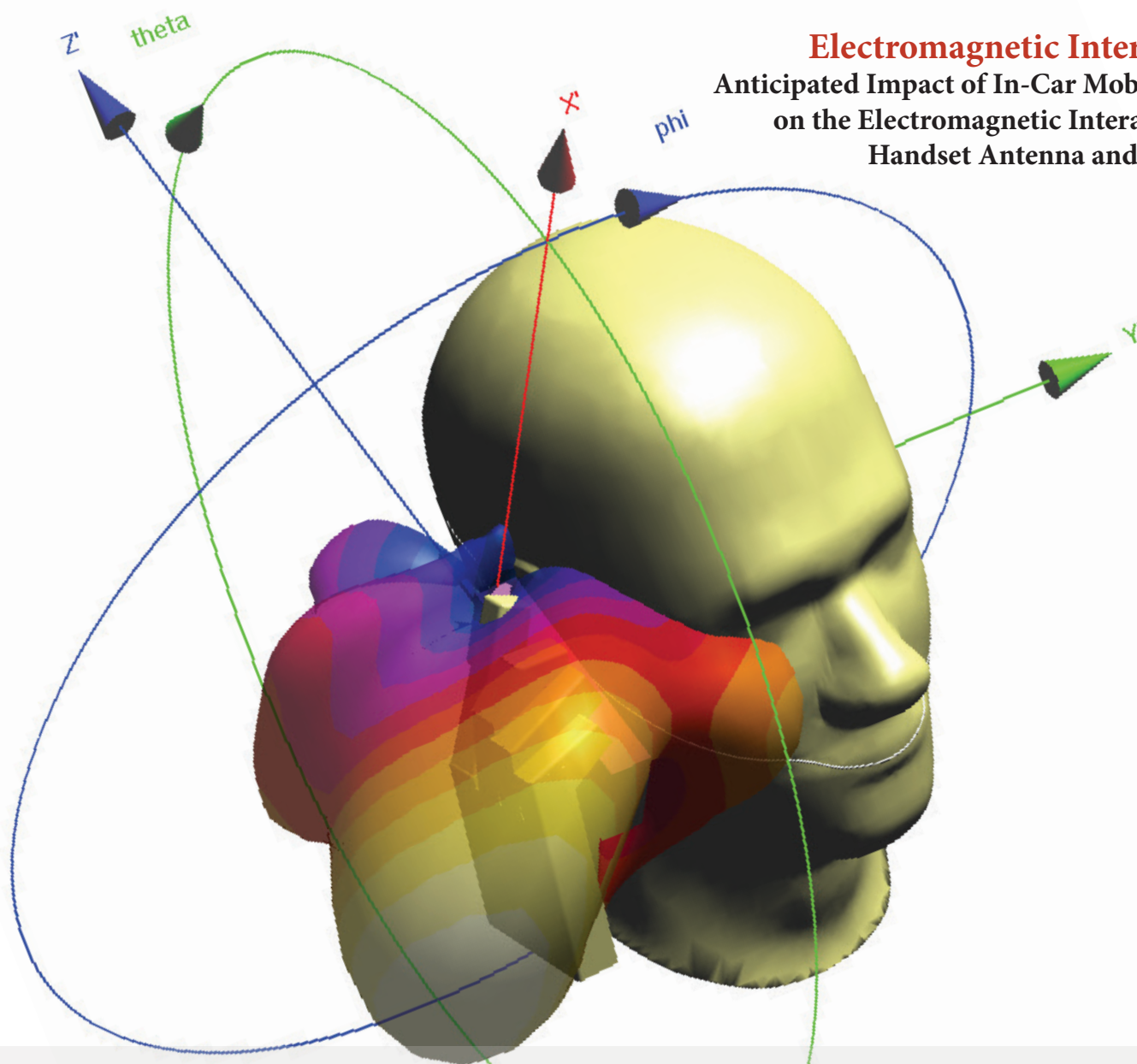


Electromagnetic Interaction

Anticipated Impact of In-Car Mobile Calls
on the Electromagnetic Interaction of
Handset Antenna and Human

Page 1



A Structural Properties of
PbS Thin Films...
Page 11

Investigations of Flare Gas
Emissions...
Page 15

A Photon Dose Enhancement
Ratio...
Page 20

Lead Removal from
Agricultural Soil...
Page 24

Non-Destructive Method for
Estimating Log Volume...
Page 32

ARO; The Scientific Journal of Koya University

The Aro ("Today" in Hewramí Kurdish), is an international scientific journal published by the Koya University with p-ISSN: 2410-9355, e-ISSN: 2307-549X and DOI: 10.14500/2307-549X. Aro is a journal of original scientific research, global news, and commentary. The Aro Scientific Journal is a peer-reviewed, open access journal that publishes original research articles as well as review articles in all areas of Science.

ARO Executive Publisher

Dr. Wali M. Hamad; is the President of Koya University and the Executive Publisher of Aro.

Aro Editorial Board

Aro's editorial board include a five-member Senior Editorial Board that helps set journal policy; a Board of Reviewing Editors consisting of more than 120 leading scientists. A complete list can be found here (<http://aro.koyauniversity.org/about/editorial-board/editorial-board>).

Aro Editorial Group

Senior Executive Editors: Dilan M. Rostam, Shwan K. Rachid, Salah I. Yahya and Sarkawt S. Abdulrahman.

This issue reviewers: Adam Narbudowicz, Adheed Sallomi, Akeel T. Al-Kazwini, Akram O. Esmail, Ali H. Ahmad, Baram A. Jaff, Francis M. Burns, Ikbal M. Gharib, Mohammed H. Sedeeq, Muataz Majeed, Mustafa S. Omer, Quirino Balzano, Salah R. Saeed and Seyd M. Sajadi.

Aro Editorial Web and New Media: Dilan M. Rostam, Salah I. Yahya and Jwan T. Rawuf

Secretary of the Journal: Jwan T. Rawuf.

Sponsorship

The cover design is sponsored by *Sadaf Kiani*, Graphic Designer/Visual Artist, Director of Studio K Design Studio based in Toronto, <http://studio-k.ca>.

Aro, the International journal of original scientific research and commentary is an online and published twice a year, as well, by Koya University. The published articles are free and online open access distributed under the Creative Commons Attribution License (<http://creativecommons.org/licenses/by/3.0/>). Responsibility of the content rests upon the authors and not upon Aro or Koya University.

ARO the Scientific Journal Office

Koya University
University Park
Danielle Mitterrand Boulevard
Koya KOY45
Kurdistan Region - F.R. Iraq

Tel.: +964(0)748 0127423

Mobile: +964(0)7502257080

E-mail: aro.journal@koyauniversity.org

url: aro.koyauniversity.org

ARO

The Scientific Journal of Koya University

Vol II, No 2(2014)

Content

Aro Editorial Words	iii
Salah I. Yahya	01
Anticipated Impact of In-Car Mobile Call on the Electromagnetic Interaction of Handset Antenna and Human	
Mohammad G. Faraj and Halo D. Omar	11
The Effect of Substrate Temperature on the Structural Properties of Spray Pyrolysed Lead Sulphide (PbS) Thin Films	
Jafar A. Ali and Loghman A. Khodakarami	15
Investigations of Flare Gas Emissions in Taq Taq Oil Field on the Surrounding Land	
Maan S. Al-Arif	20
Photon Dose Enhancement Ratio at the Transition Region of Dissimilar Media	
Karzan A. Omar and Nisar S. Omar	24
Lead Removal from Agricultural Soil of Kurdistan Region by Fe ₃ O ₄ Nanoparticles	
Talat M. Amin	32
Non-Destructive Method for Estimating Log Volume for Melia Azedarach L. Trees in Erbil-Iraqi Kurdistan Region	
General Information	37
Guide to Author	38
ARO Reviewer/Associate Editor Application Form	40



Aro Editorial Words

You are now holding Vol 2, No 2 of Aro the Scientific Journal of Koya University. Aro is now with the second year of its journey and it will continue to become a globally recognized scientific journal with wider local impact. The editorial team is determined to keep the path of such a mission and sustain Aro's future publications with quality in mind.

Aro was created with a long-term visions of becoming accessible to all researchers in Kurdistan and beyond, and covering a wide range of scholarly disciplines in sciences. The focus of the journal is to reflect that of the Koya University, namely promoting scientific knowledge and research in Kurdistan and secure a brighter future in education. Aro aspires to become a channel for exchange of scholarly research by establishing academic connections between scholars.

Aro is a journal of original scientific research, global news, and commentary. The Aro Scientific Journal is a peer-reviewed, open access journal that publishes original research articles as well as review articles in areas of natural sciences and technology. In this issue you will have access to genuine research paper in variety of areas, such as biochemistry, engineering and material.

Aro is a member of CrossRef, which is a not-for-profit membership association whose mission is to enable easy identification and use of trustworthy electronic content by promoting the cooperative development and application of a sustainable infrastructure. Beside its online publications, Aro has a semi-annual hard copy publication which is available free-of-charge.

The warm response from researchers, academics and professionals made our task of creating an editorial board a relatively easy one. It is clear that having a dedicated and well organized editorial board for the journal is only one side of the coin. The other is the ability to attract submissions of quality research and scholarly work. We are thankful to all of those who put their trust in Aro and presented their original research work for publication in Vol 2, No 2 of the journal, as well as, our thanks are extended to the fourteen peer-reviewers from the universities worldwide for their efforts in reviewing this issue of Aro publications.

Your support and feedback are invited and appreciated.

Sincerely

Wali M. Hamad
Executive Publisher

Dilan M. Rostam, Shwan K. Rachid, Salah I. Yahya and Sarkawt S. Abdulrahman
Executive Editorial Board

Anticipated Impact of In-Car Mobile Calls on the Electromagnetic Interaction of Handset Antenna and Human

Salah I. Yahya

Department of Software Engineering, Faculty of Engineering, Koya University
University Park, Danielle Mitterrand Boulevard, Koya KOY45, Kurdistan Region of F.R. Iraq

Abstract—This paper investigates the impact of the in-car mobile call on the electromagnetic interaction of the mobile handset antenna and user's head. This impact was evaluated from two different perspectives; First, the antenna performance, e.g., total isotropic sensitivity and total efficiency, and second, the specific absorption rate (SAR) induced in the user's head. A Yee-FDTD based electromagnetic solver was used to simulate a mobile phone in hand close proximity to head at cheek and tilt positions, and working at a frequency of 1900 MHz (GSM 1900/PCS) while making a call inside a car. A Specific Anthropomorphic Mannequin (SAM) was used to simulate the user's head, a generic phone was used to simulate the mobile phone, a semi-realistic model with three tissues, i.e., skin, bone and muscle, was used to simulate the user's hand, and a CAD model of Ferrari F430-brand was used to simulate the car. The results showed a considerable degradation in the mobile phone antenna performance while making a mobile phone call inside a car that may drive the mobile phone increases its radiated power to establish a successful connection with the base-station antenna, and consequently increases the induced specific absorption rate in the user's head.

Index Terms—Antenna efficiency, FDTD, mobile phone antenna, phantom, specific absorption rate (SAR), specific anthropomorphic mannequin (SAM), TIS.

I. INTRODUCTION

The possible health hazard of cellular communication handsets due to their electromagnetic (EM) interaction with human have been investigated during the last twenty years, (Toftgard, Hornsleth, and Andersen, 1993; Dimbylow and Mann, 1994; Gandhi, Lazzi and Furse, 1996; Watanabe, et al., 1996; Abousetta, et al., 1999; Francavilla, et al., 2001; Wang

and Fujiwara, 2003; Chavannes, et al., 2006; Kouveliotis, et al., 2006; Futter, et al., 2008; Al-Mously and Abousetta, 2008a; Al-Mously and Abousetta, 2008b; Al-Mously and Abousetta, 2008c; Al-Mously and Abdalla, 2009; Al-Mously and Abousetta, 2009a; Al-Mously and Abousetta, 2009b; Al-Mously, 2011a; Al-Mously, 2011b; Al-Mously, 2012a; Al-Mously, 2012b). This hazard is varied based on position of handset with respect to user's head and also the hand position that holding the handset. Beside this hazard, a degradation in the handset antenna performance, i.e., total isotropic sensitivity (TIS) and total efficiency (η_{tot}) are expected and may lead to a low handset antenna power radiation in some circumstances. Consequently, the handset increases the radiated power to maintain a successful call that will certainly increase the specific absorption rate (SAR) induced in the user's head and then increases the radiation hazard.

The influence of the metallic structures of a car body frame on the SAR produced by a cell phone when a complete human body model is placed at different locations inside the vehicle was analyzed by Anzaldi, et al. (2007). A dipole antenna at 835 MHz located as a hands-free communication device was modeled to simulate the mobile phone.

The impact of source location and human occupancy configurations on in-vehicle SAR levels due to 400 and 900 MHz on board transmitters was investigated using numerical models by Ruddle (2007; 2009).

The SAR evaluation in the scenarios of passengers using different wireless communication devices inside a vehicle was evaluated by Diao (2013). The effects of the devices with different operational frequencies 900MHz/1.8GHz/2.4GHz, and different seating locations on the SARs were investigated. A simple metal frame was used to simulate the vehicle. A block model for the body and sphere model for the head were used to simulate the human complete body. The generic phone was used in a vertical position and placed in close vicinity to head, but not according to the recommended positions by the IEEE (IEEE-Std. 1528, 2003), i.e., check and tilt.

None of the publications (Anzaldi, 2007; Ruddle, 2007, 2009; Diao, 2013) used a complete realistic car model including all parts, and the mobile phone model was not grabbed by hand and placed in close vicinity to head

according to IEEE standard (IEEE-Std. 1528, 2003). Moreover, the impact while making a mobile call inside a car on the handset antenna performance was not investigated too.

This paper tries to investigate the EM interaction of a handset antenna and user's head while making a call inside a car. This can be achieved by evaluating the handset antenna performance degradation and the amount of the SAR induced in the user's head. Handset TIS and η_{tot} , and induced SAR in the user's head were all evaluated for holding a handset close proximity to head at cheek and tilt-position while making a call inside a complete realistic car model. The numerical calculation is based on Yee-FDTD technique using SEMCAD X version 14.0 Altesch (Schmid & Partner Eng. AG, 2009).

The reminder of the paper is organized as follow. In Section II, the FDTD-based numerical method is described, In Section III, the design models involved in the numerical computations are styled. In Section IV, the FDTD grid generation needed to realize the study case using FDTD method is given. In Section V, the adopted computation technique results are validated in comparison with previous published work results. In Section VI, the results and implications are illustrated. Section VII discusses the results. Section VIII gives the computational requirements. Finally, section IX concludes the paper.

II. THE FDTD-BASED NUMERICAL METHOD

The Finite-Difference Time-Domain (FDTD) method that proposed by Yee (1966) is adopted in this paper as a numerical computation to solve a Maxwell's curl equations in the time domain. Maxwell's curl equations in the time domain are:

$$\nabla \times \mathbf{E} = -\frac{\partial}{\partial t} \mu \mathbf{H} - \sigma_H \mathbf{H} \quad (1)$$

$$\nabla \times \mathbf{H} = \frac{\partial}{\partial t} \varepsilon \mathbf{E} + \sigma_E \mathbf{E} \quad (2)$$

$$\mathbf{E} = \begin{pmatrix} E_x \\ E_y \\ E_z \end{pmatrix}, \quad \mathbf{H} = \begin{pmatrix} H_x \\ H_y \\ H_z \end{pmatrix} \quad (3)$$

where ε and μ are the electric and magnetic properties, of the material, and σ_E and σ_H are the electric and magnetic conductivity, respectively. Maxwell's curl equations are discretized using a 2nd order finite-difference approximation both in space and in time in an equidistantly spaced mesh (Schmid & Partner Engineering AG, 2009). The SEMCAD-X simulation platform is selected for simulating the study cases in this work due to its handling, functionality and features for highly detailed CAD models as well as efficient FDTD solver for simulating advanced applications.

III. DESIGN MODELS

A. Handset Design Model

Different generic phone models were suggested to simulate

the mobile phone (IEEE-Std. 1528, 2003; Beard, et al., 2006; Al-Mously and Abousetta, 2008d). The one which suggested by Beard, et al. (2006) and shown in Fig. 1 was adopted and used to simulate the mobile phone handset for the sake of computation technique verification/validation.

Due to the huge amount of FDTD cells needed to simulate a phone call session inside a car, only a working frequency at 1900 MHz that represent the GSM-1900/PCS was used. This 1900 MHz is near the operating frequency of the GSM-1800 MHz. The antenna length is 36 mm and its square cross section has a 1-mm edge. The monopole is coated by a 1 mm thick plastic having permittivity $\varepsilon_r = 2.5$ and electrical conductivity $\sigma = 0.005 \text{ S/m}$. The chassis comprised a PCB, having lateral dimensions of 40×100 mm and a thickness of 1 mm, symmetrically embedded in a solid plastic case with permittivity $\varepsilon_r = 4.0$ and electrical conductivity $\sigma = 0.04 \text{ S/m}$, lateral dimensions 42×102 mm, and thickness 21 mm. The antenna is mounted along the chassis centerline so as to avoid differences between right- and left-side head exposure. The antenna is a thick-wire model whose excitation was a $50 - \Omega$ sinusoidal voltage source at the gap between the antenna and PCB.

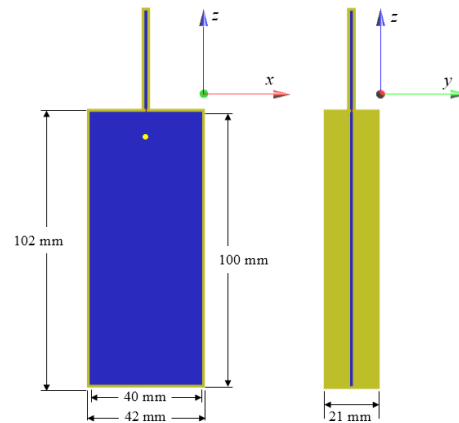


Fig. 1. The CAD model with dimensions of the generic phone used to simulate the mobile phone handset.

B. User's Hand Model

A semi-realistic hand model consisting of three tissues; skin, muscle and bone (Al-Mously and Abousetta, 2008a; 2009b) was designed and used to simulate the user's hand holding the cellular handset. Table I lists the dielectric properties of the three hand tissues.

C. User's Head Model

A Specific Anthropomorphic Mannequin (SAM) developed by different standard committees (IEEE Standard 1528–2003, 2003; IEC 62209-1, 2005) and represents the world-wide standard phantom for compliance testing is used to simulate the human head. The electrical properties of the SAM materials are defined as shown in Table I (IEEE Standard 1528–2003, 2003; IEC 62209-1, 2005; Beard, et al., 2006).

TABLE I
THE MAIN DIELECTRIC PARTS OF THE HAND AND SAM TISSUES, AND THE CORRESPONDING MATERIAL PARAMETERS

Hand Tissue	ϵ_r	σ (S/m)	ρ (kg/m ³)
Hand skin	38.714	1.2245	1100
Hand muscle	53.418	1.3963	1041
Hand bone	11.716	0.2924	1990
SAM Tissue	ϵ_r	σ (S/m)	ρ (kg/m ³)
SAM shell	5.00	0.0016	1030
SAM liquid	40.0	1.40	1030

D. Car Model

A CAD-model for Ferrari F430-brand available with (Schmid & Partner Engineering AG, 2009) is used to simulate the car. The exact Ferrari F430 measured dimensions are; 4512 mm (equal to 177.6 in) length, 1923 mm (75.7 in) width and 1234 mm (48.6 inches) height (Ferrari, 2014), whereas, the dimensions of the F430 CAD model are; 4480 mm length, 1980 mm width and 1204 mm height, which are almost the same. Four different materials were recognized in the CAD model to simulate all car-materials; metal, plastic, glass and leather.

Ferrari F430-brand may effect on the mobile phone antenna EM wave radiation like any other sedan automobile, it has been chosen because the Ferrari CAD model is already available commercially. Fig. 2 shows the Ferrari-F430 CAD model.

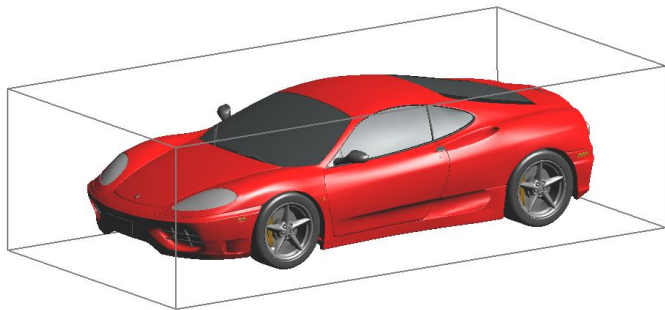


Fig. 2. The CAD model of the Ferrari F430-brand car.

IV. FDTD GRID GENERATION

Six different scenarios were considered to anticipate the EM interaction of the handset antenna and user’s head while setting a mobile call inside a car;

1. Handset, without user’s hand, close proximity to head at cheek-position making a mobile call in free-space.
2. Handset, without user’s hand, close proximity to head at tilt-position (15°) making a mobile call in free-space.
3. Handset in hand and close proximity to head at check-position making a mobile call in free space.

4. Handset in hand and close proximity to head at tilt-position making a mobile call in free space.
5. Handset in hand and close proximity to head at check-position making a mobile call inside a car.
6. Handset in hand and close proximity to head at tilt-position making a mobile call inside a car.

It is important to mention that the procedure for the evaluation of the Electromagnetic (EM) interaction between the mobile phone antenna and human body presented by Al-Mously (2011b) is adopted and followed in this paper. The FDTD grid cells were aligned in the direction of handset antenna, e.g. the cells are parallel and in the z-direction.

A. Grid Generation of the Scenarios 1 and 2

In these two scenarios a handset close proximity to head at cheek and tilt-position making a mobile call in free-space were set and modeled. The purpose of these two scenarios is to validate the FDTD numerical computation by comparing the achieved results in this paper with the results given by Beard, et al. (2006). A minimum spatial resolution of 1×1×1 mm³ and a maximum spatial resolution of 3×3×3 mm³ in the x, y, and z directions are chosen for simulation. The absorbing boundary conditions (ABCs) are set as a uniaxial perfectly matched layer (UPML) mode with a very high strength thickness, where minimum level of absorption at the outer boundary is (>99.9%). A grading ratio of 1.2 is used for the solid regions during the simulations. Fig. 3 shows the CAD models of both scenarios.

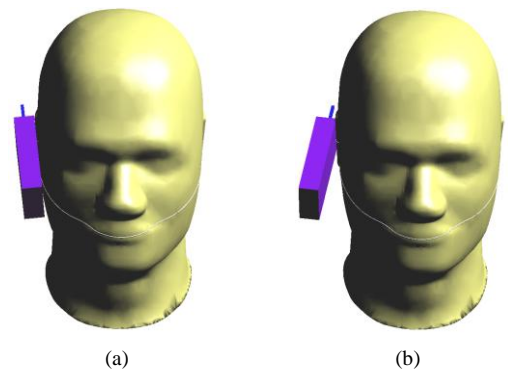


Fig. 3. The CAD representation of the handset close proximity to head (SAM); (a) at cheek-position and (b) at tilt-position (15°).

B. Grid Generation of the Scenarios 3 and 4

For the scenarios 3 and 4, a minimum spatial resolution of 1×1×1 mm³ and a maximum spatial resolution of 3×3×3 mm³ in the x, y, and z directions are chosen for simulation. The absorbing boundary conditions (ABCs) are set as a uniaxial perfectly matched layer (UPML) mode with a very high strength thickness, where minimum level of absorption at the outer boundary is (>99.9%). A grading ratio of 1.2 is used for the solid regions during the simulations. Fig. 4 shows the CAD models of both scenarios.

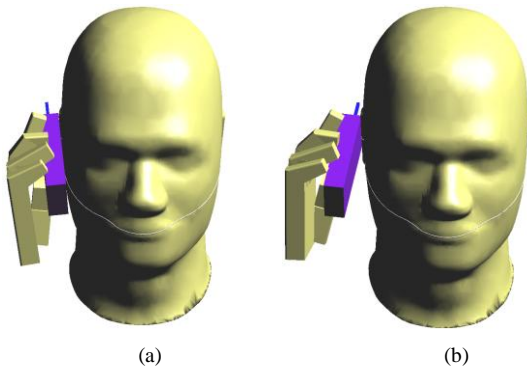


Fig. 4. The CAD representation of the handset in hand close proximity to head (SAM); (a) at cheek-position and (b) at tilt-position (15°).

C. Grid Generation of the Scenarios 5 and 6

For the scenarios 5 and 6, a minimum spatial resolution of $1 \times 1 \times 1 \text{ mm}^3$. The lowest number of cells per wavelength was 4 which gives reasonable results (Dimbylow and Gandhi, 1991). A grading ratio of 1.3 is used for the solid regions during the simulations. Same boundary conditions of Scenario 3 and 4 were used in this scenario. For the six scenarios, a 15 simulation cycles were set to achieve stability.

Fig. 5 shows the CAD models of the scenarios 5 and 6, whereas, Fig. 6 shows the visualization of voxels after gridding of the scenario 5, where the grid-cells are aligned with handset antenna dimensions, not the car dimensions.



Fig. 5. The CAD representation of the handset in hand close proximity to head; (a) While making a mobile call inside a car at cheek-position and (b) While making a mobile call inside a car at tilt-position.

Table II lists the total number of FDTD-grid cells required to simulate the handset models in all six scenarios.

TABLE II
THE NUMBER OF GRID CELLS (IN MCELL) GENERATED USING FDTD METHOD FOR THE DIFFERENT SCENARIOS AT 1900 MHZ

Number of FDTD grid cells (Mcell) with simulation time (hh:mm:ss)	Cheek-position	Tilt-position
Handset close proximity to head while making a call in free space, without hand.	2.45522 00:05:12	2.46208 00:05:26
Handset in hand close proximity to head while making a call in free space.	3.42624 00:07:02	3.26771 00:06:23
Handset in hand close proximity to head while making a call inside a car.	29.7216 02:17:00	26.576 02:03:00

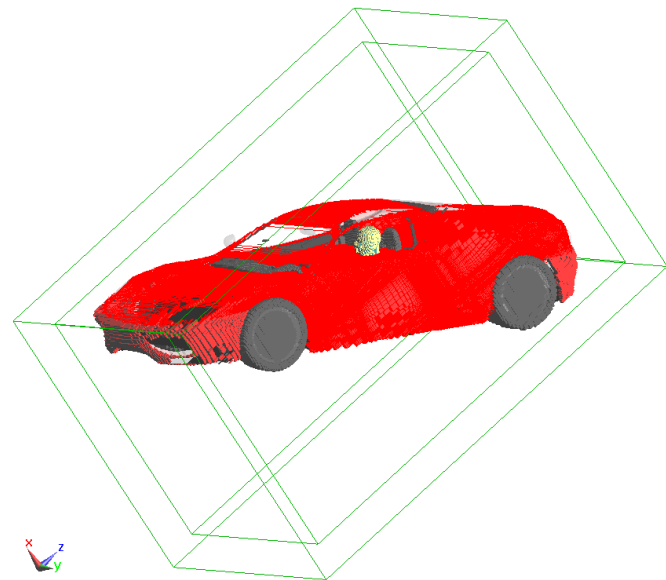


Fig. 6. Visualization of voxels after gridding. Cheek-position and grid of (29.72160) Mcell.

V. VALIDATION OF THE COMPUTATION TECHNIQUE

To validate the numerical computation and the FDTD-method adopted in this paper, a comparison with other published results using a same scenario is essential. The validation of the adopted FDTD computation was achieved by comparing the results of scenarios 1 and 2 with the results given by Beard, et al. (2006) for the same scenarios, where a handset close proximity to head at cheek and tilt-position in free space were modeled as shown in Fig. 3. Table III gives the computed induced SAR in head and the one given by Beard, et al. (2006) for the handset close proximity to head at both cheek and tilt-position with antenna input power of 1.0 Watt. Both results at each position show a good agreement and validate the adopted numerical computations of this paper.

TABLE III
THE COMPUTED SAR_{1g} INDUCED IN HEAD AND THE ONE CALCULATED BY BEARD, ET AL. (2006) FOR THE HANDSET CLOSE PROXIMITY TO HEAD AT CHEEK AND TILT-POSITION, AND IN FREE-SPACE. BOTH RESULTS ARE NORMALIZED TO 1 W INPUT POWER

	Position	¹ SAR _{1g} (W/kg)	² SAR _{1g} (W/kg)
Handset close proximity to head making a call in free-space (no hand is involved)	<i>Cheek</i>	8.28	8.27
	<i>Tilt</i>	11.97	11.97

1 The computation obtained by Beard, et al., (2006).

2 The computation obtained in this work.

VI. RESULTS AND IMPLICATIONS

The impact of in-car mobile phone call on the electromagnetic interaction of the handset antenna and user's head was evaluated from two different perspectives; first, the

antenna performance, second, the specific absorption rate (SAR) induced in the user's head

The antenna performance represented by the antenna total efficiency (η_{tot}), total radiated power (TRP) and total isotropic sensitivity (TIS). Both TRP and η_{tot} are defined as follow (Balanis, 1997);

$$TRP = \eta_{tot} \times \text{input power} \quad (4)$$

$$\eta_{tot} = \eta_{rad} \times \eta_{mis} \quad (5)$$

where (η_{rad}) is the radiation efficiency and (η_{mis}) is the mismatch efficiency.

The TIS is a measure of the handset receiving performance, where both TIS and TRP together determine the effectiveness of the handset as a piece of radio equipment, in particular the maximum range at which the handset can operate from the base station with some given level of performance (Chen, 2007).

The specific absorption rate (SAR) induced in the user's head is an index that quantifies the rate of energy absorption in biological tissue expressed in watts per kilogram (W/kg). SAR is generally quoted as a figure averaged over a volume corresponding to either 1 g or 10 g of body tissue. Based on SCC-34, SC-2, WG-2 - Computational Dosimetry, IEEE-Std. 1529 IEEE Standard-1529, draft), an algorithm has been implemented using a FDTD-based EM simulator, SEMCAD X (Schmid & Partner Engineering AG, 2009).

The handset in all six scenarios is modeled with operating frequency of 1900 MHz and antenna input power of 125 mW.

The antenna performance parameters η_{mis} , η_{rad} and η_{tot} given for the handset making a call in free space, making a call while in hand close to head in free space and making a call while in hand close to head inside a car are all listed in Table IV, whereas, the total radiated power (TRP), TIS and induced SAR (averaged over 1g) in head values are listed in Table V.

TABLE IV

THE ANTENNA EFFICIENCIES OF THE HANDSET IN DIFFERENT SCENARIOS

	$\eta_{mis}\%$	$\eta_{rad}\%$	$\eta_{tot}\%$
Handset with a call in free-space	88.07	92.33	81.32
Handset in hand close proximity to head while making a call in free space	89.26	24.89	22.21
	96.50	23.78	22.95
Handset in hand close proximity to head while making a call inside a car	80.75	0.844	0.682
	47.77	1.112	0.532

The values of the induced SAR_{1g} in head for both cheek and tilt positions and listed in Table V are almost under the limit of the IEEE/ANSI/FCC (IEEE-Std. C95.1b, 2004; IEEE Standard-1529, draft), where the maximum is 1.6 (W/kg) averaged over 1g.

Fig. 7 illustrates the 3D electrical far-field radiation pattern

of the handset in hand close proximity to head at cheek-position while making a call in free-space. The same radiation pattern is illustrated in Fig. 8, but for the handset at tilt-position.

TABLE V

THE ANTENNA TRP AND TIS OF THE HANDSET AT DIFFERENT SCENARIOS WITH THE CORRESPONDING SAR_{1g} INDUCED IN HEAD AT 1900 MHz

	TRP mW	TIS dBm	SAR _{1g} W/kg
Handset with a call in free-space	101.65	-105	na
Handset in hand close proximity to head while making a call in free space	27.00	-99.48	1.06
	28.69	-99.63	1.63
Handset in hand close proximity to head while making a call inside a car	0.85	-84.36	1.06
	0.66	-83.27	1.68

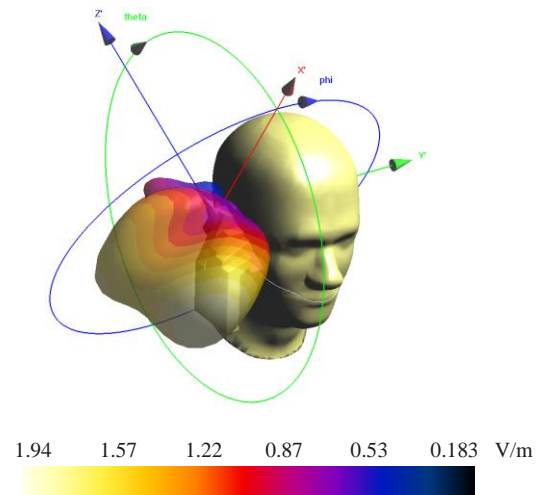


Fig. 7. The three-dimensional electrical far-field radiation pattern of the handset in hand close to head at cheek-position while making a call in free-space.

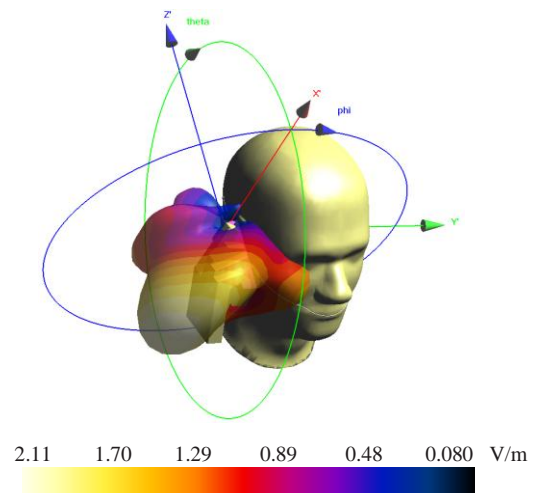


Fig. 8. The three-dimensional electrical far-field radiation pattern of the handset in hand close to head at tilt-position while making a call in free-space.

Fig. 9-a shows the surface distribution of the spatial peak SAR [IEEE-1529] for the handset in hand close proximity to head at cheek-position while making a call inside a car. Fig. 9-b shows the same distribution at cheek-position with zoomed head view, whereas, Fig. 9-c shows the same distribution at tilt-position.

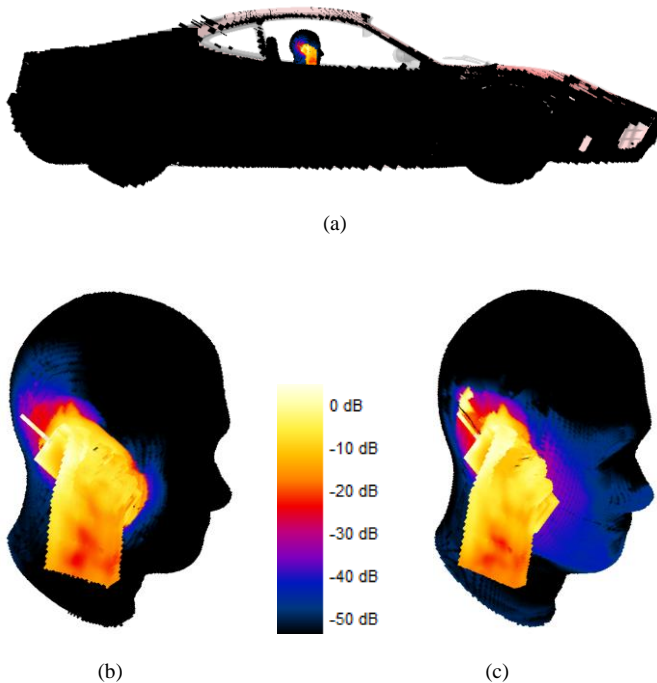


Fig. 9. The spatial peak SAR [IEEE-1529] surface distribution for the handset in hand close proximity to head at cheek-position while making a call inside a car, (b) the same surface distribution for the zoomed head at cheek-position, and (c) the same surface distribution for the zoomed head at tilt-position.

Fig. 10 shows the handset in hand close proximity to head inside a car with x , y , z axis and θ and ϕ directions to illustrate the 3D far-field radiation patterns of the handset inside a car while making a mobile call at cheek and tilt-position, Fig. 11 and Fig. 12, respectively.

The 3D electrical far-field radiation pattern of the handset inside a car at cheek-position, Fig. 11, shows a dramatic radiation pattern change, as compared with the patterns of Fig. 7 and Fig. 8. The main lobe is the direction of the car roof due to the ground effect with minor lobes in the left-side direction of the driver, whereas, Fig. 12 shows two main lobes, one in the direction of the car roof and the other in the left-side direction of the driver due to tilting the handset 15° with respect to head

VII. DISCUSSION

A. Unsuccessful Mobile Call Establishment inside a Car

The results given in Table IV shows a high degradation in the antenna performance, i.e., η_{tot} , of the handset in hand

close proximity to head while making a mobile call inside a car, as compared with the case in free space. A degradation of (-96.9%) at cheek-position and (-97.7%) at tilt-position are observed. This is mainly due to the degradation in the η_{rad} because of the car body coverage, and degradation in the η_{mis} , as well. Although the presence of head at both positions in free space degrades the antenna η_{rad} but at the same time it improves the antenna η_{mis} , Table IV. On the other hand, this improvement turns oppositely when the antenna is placed close to head and directly under the car metal roof, especially at tilt position where the antenna is closer to head. (-9.5%) degradation in the antenna η_{mis} at cheek position was noticed, whereas, a (-50.5%) degradation was at tilt position.

The same scenario of degradation was observed, Table V, for the TIS while making a mobile call inside a car, as compared with the call in free space. A degradation of (-15.2%) and (-16.4%) was computed for the cheek and tilt-position, respectively. It is obvious that the presence of car shows more negative impact on the handset antenna performance at tilt-position, as compared with the case at cheek-position. The same effect is applicable for the TRP , Table V, since TRP depends directly on the η_{tot} , (4).

Table V shows that the induced SAR_{1g} in the user's head at tilt-position is more than at cheek-position, while making a call in free-space. These results are in consistency with the results presented by Al-Mously and Abousetta (2008b).

Since the SAR_{1g} induced in the user's head depends on the handset antenna near field, not the far field radiation, the multi reflections of the handset EM waves inside a car should have no effect on the amount of the induced SAR_{1g} . For the same antenna input power (125 mW) of the handset making a call in free-space and inside a car, as well, no change in the SAR_{1g} values were noticed due to the presence of car, as shown in Table V.

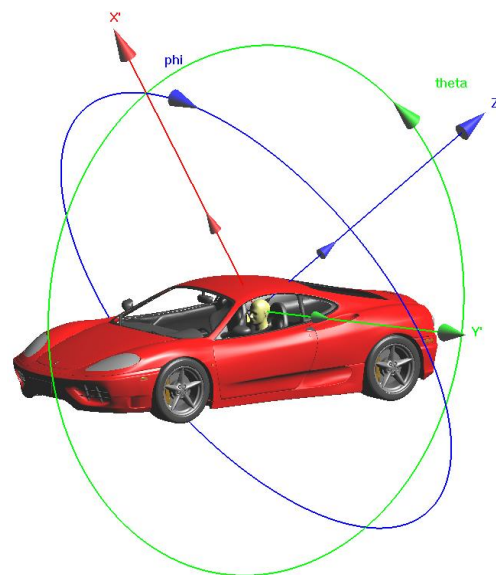


Fig. 10. The CAD model of the handset in hand close proximity to head inside a car with x , y , z axis and θ and ϕ directions.

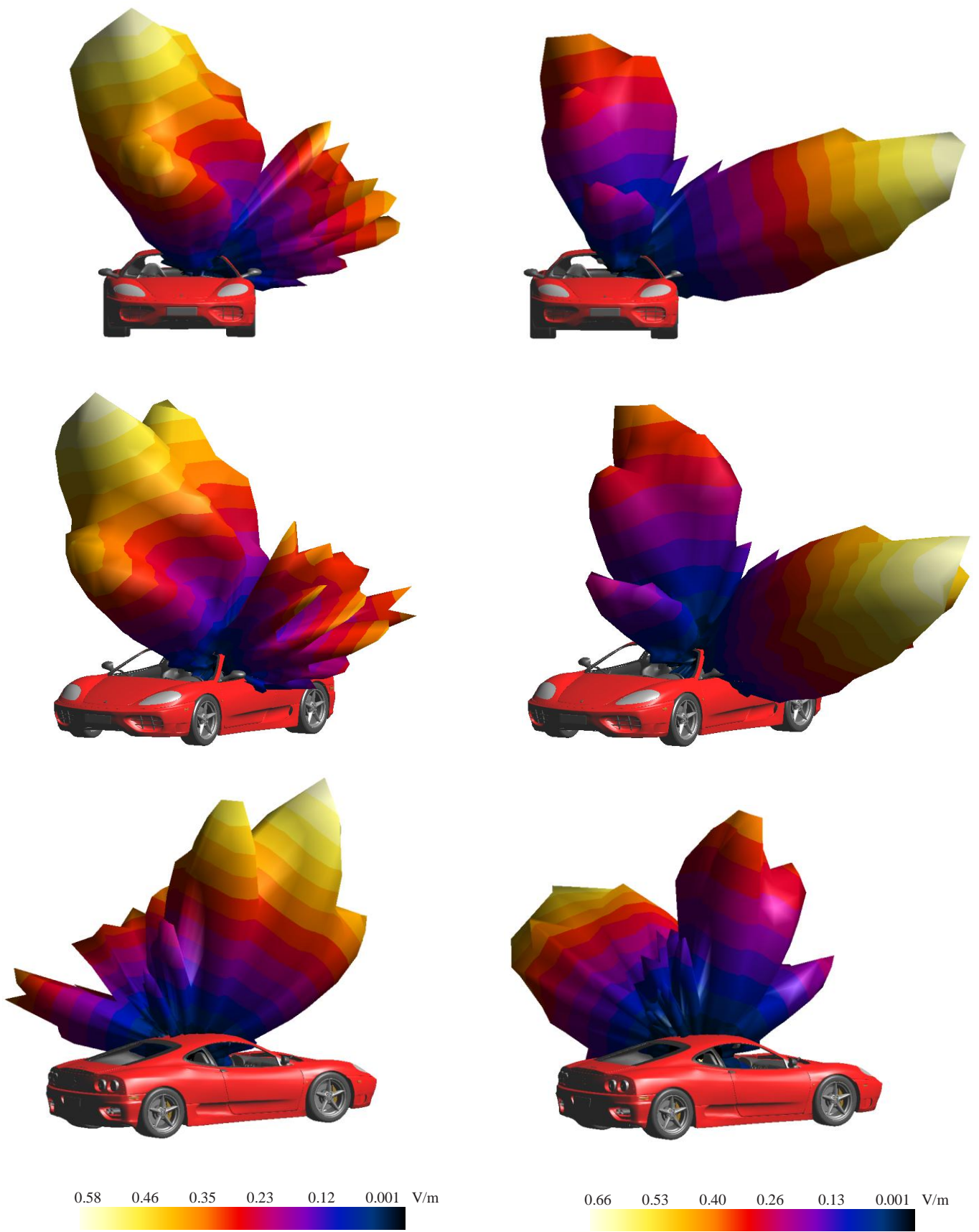


Fig. 11. Different views of the 3D total electric radiation pattern of the handset in hand close proximity to head at cheek-position while making a mobile call inside a car.

Fig. 12. Different views of the 3D total electric radiation pattern of the handset in hand close proximity to head at tilt-position while making a mobile call inside a car.

According to (4) and with antenna TIP of 125 mW, the antenna TRP is 0.85 mW for the handset at check-position and 0.66 mW for the handset at tilt-position, while making a mobile call inside a car, Table VI. These $TRPs$ are not enough to establish a successful call with the mobile base-station antenna, The mobile base-station needs a minimum of 1 mW (0.0 dB), power level number 15, to be connected successfully with the handset terminal (Poole, 2004).

The recommended minimum accepted degradation in TIS while making a mobile call, as compared with the mobile call in free-space, neither hand nor head proximity exists, is about 10-12 dBm (Lindberg, 2007; Al-Mously and Abousetta, 2009a). This recommendation does exist with the handset while making a call in free-space, but does not exist while making a mobile call inside a car, Table V. Moreover, the recommended minimum accepted TIS for the GSM family is – (92.4 - 99.4) dBm, based on frequency (Pedersen, 2012), regardless the handset position or the object in close proximity. Also, this recommendation does exist with the handset while making a call in free-space, but does not exist while making a mobile call inside a car, where the TIS values are -84.36 and -83.27 for cheek and tilt-position with degradation of -20.64 dBm and -21.73 dBm, respectively, Table V.

Therefore, the unaffected safely SAR_{1g} values that given in Table V due to the presence of car are considered not realistic and do not reflect the actual values, as long as a successful connection between the handset of such a scenario with a mobile base-station cannot be established due to low TRP .

B. Successful Mobile Call Establishment inside a Car

As mentioned above, the establishment of a successful call between the handset and mobile base-station necessitates a TRP of more than 1 mW. Based on the TRP values given in Table V, for the handset making a call inside a car, the mobile base-station sends a signal to handset requests for increasing the antenna output power which consequently increases TIP . Table VI shows that the increments of 17.6% and 51.5% in the TRP , for cheek and tilt-position, respectively, are required to achieve the minimum value of 1 mW. These increments necessitate a corresponding increments in the TIP . $TIPs$ of 147.1 mW and 189.4 mW are looked-for to achieve a successful mobile call.

TABLE VI
THE ACTUAL TRP AND LOOKED-FOR TIP VALUES FOR THE HANDSET IN SCENARIOS 5 AND 6

		¹ TRP mW	² TRP mW	³ Incr. %	⁴ TIP mW
Handset in hand close proximity to head while making a call inside a car	<i>Cheek</i>	0.85	1.00	17.6	147.1
	<i>Tilt</i>	0.66	1.00	51.5	189.4

1 The actual TRP that establishes an unsuccessful mobile call.

2 The minimum TRP required to establish a successful mobile call.

3 Increment percent in TRP to establish a successful mobile call.

4 The looked-for corresponding TIP for a successful mobile call.

With these new TIP values, which represent the minimum looked-for values and able to establish a successful mobile call, the numerical computation of the scenarios 5 and 6 were scaled accordingly, since the SAR is directly proportional with the input power. The handset antenna TIP is set to equal 147.1 mW for the scenario 5 and 189.4 mW for the scenario 6, instead of the 125 mW for both. The corresponding new TRP and SAR_{1g} values were achieved and listed in Table VII. The numerical computation shows TRP of 1 mW for both scenario, 5 and 6. Thus the corresponding SAR values induced in the user's head can be considered realistic as long as with such TIP and TRP values a mobile call between the mobile base-station and the handset terminal can be established successfully.

TABLE VII
THE MINIMUM LOOKED-FOR TIP VALUES FOR ESTABLISHING A SUCCESSFUL MOBILE CALL INSIDE A CAR AND THE CORRESPONDING TRP AND SAR VALUES AT DIFFERENT POSITIONS.

	¹ TIP mW	TRP mW	SAR_{1g} W/kg
Handset in hand close proximity to head while making a call inside a car	147.1	1.00	1.25
<i>Cheek</i>			
<i>Tilt</i>	189.4	1.00	2.54

1 The minimum looked-for TIP corresponding to a successful mobile call.

It is very clear in Table VII that establishing a successful mobile call inside a car which necessitates a TIP increment that consequently leads to increase the induced SAR_{1g} in head by percent values of 17.6% and 51.5% at cheek and tilt-position, respectively. Due to this increase, the SAR_{1g} may cross the IEEE/ANSI/FCC limits as in the case of tilt-position, 2.54 W/kg.

VIII. COMPUTATIONAL REQUIREMENTS

All computations were performed on a CPU of 2.4 GHz Intel® core™ i7 Laptop machine (Dell, XPS L702X) with 8 GB memory and 64-bit Windows operating system. No hardware accelerator aXware (Schmid & Partner Engineering AG, 2009) was used to accelerate the simulations. The number of FDTD grid cells and running time were totally depend on the problem size.

IX. CONCLUSION

In addition to the continuous calling of the national transportation safety boards and agencies in most countries for a complete ban on talking by mobile phone while driving, due to the possible car accidents, this paper showed a possible biological hazard of the mobile call inside a car or while driving owing to the induced SAR in head tissues. The results achieved throughout this paper showed a significant degradation in the handset antenna performance, i.e., total isotropic sensitivity and total efficiency, while making a

mobile call inside a car. This degradation may not initiate the handset to establish a successful mobile call and consequently the mobile base-station may request the handset to increase its input power. Accordingly, this will certainly increase the induced SAR in head. The numerical computations showed a 17.6% and 51.5% increase in the spatial peak SAR_{1g} induced in the head tissues for the handset at cheek and tilt-position, respectively, while making a mobile call inside a car, as compared with the mobile call in free space. In other words, making a mobile phone call inside a car is more hazardous than a mobile call in free space and the SAR_{1g} induced in head tissues may cross the IEEE/ANSI/FCC standard limits.

REFERENCES

- Abousetta, M.M., Alhamdani, Z.K., Al-Mously, S.I., Al-Daghistani, M.E., Omran, K.F., 1999. Electromagnetic hazard mitigation in mobile telephones. In: IEE, *Seminar on electromagnetic assessment and antenna design relating to health implications of mobile phones* (Ref. No. 1999/043), June 1999. London, UK.
- Al-Mously, S.I., 2011a. Factors influencing the EM interaction between mobile phone antennas and human head. *Digital Information and Communication Technology and its Applications Communications in Computer and Information Science*, 166, pp.106-120.
- Al-Mously, S.I., 2011b. Assessment procedure of the EM Interaction between mobile phone antennae and human body. *International Journal on New Computer Architectures and Their Applications (IJNCAA)*, 1(1), pp.1-14.
- Al-Mously, S.I., 2012a. Mobile phone EMC deterioration due to different realistic usage patterns. In: PIER, *Progress in electromagnetics research symposium*, August 2012. Moscow, Russia.
- Al-Mously, S.I., 2012b. *Cellular handset antennas design, performance enhancement, and assessment of their EM interaction with a human*, 1st ed. LAP Lambert Academic Publishing, ISBN: 978-3-8473-0403-6
- Al-Mously, S.I., Abdalla, A.Z., 2009. Hand implications on the coupling between human head and different cellular phones. In: TELSIKS, *9th International conference on telecommunication in modern satellite, cable, and broadcasting services*, 7-9 Oct. 2009. Serbia, Belgrade.
- Al-Mously, S.I. and Abousetta, M.M., 2008a. A novel cellular handset design for an enhanced antenna performance and a reduced SAR in the human head, *International Journal of Antennas and Propagation*, 10 pages. doi:10.1155/2008/642572
- Al-Mously, S.I. and Abousetta, M.M., 2008b. Anticipated impact of hand-hold position on the electromagnetic interaction of different antenna types/positions and a Human in cellular communications, *International Journal of Antennas and Propagation*, 22 pages. doi:10.1155/2008/102759
- Al-Mously, S.I. and Abousetta, M.M., 2008c. A Study of the Hand-Hold Impact on the EM Interaction of a Cellular Handset and a Human, *International Journal of Electronics, Circuits and Systems*, 2(2), pp.91-95.
- Al-Mously, S.I. and Abousetta, M.M., 2008d. Study of both antenna and PCB positions effect on the coupling between the cellular hand-set and human head at GSM-900 standard. In: IWAT2008, *The international workshop on antenna technology*, 4-6 March 2008. Chiba University, Japan.
- Al-Mously, S.I. and Abousetta, M.M., 2009a. User's Hand Effect on TIS of Different GSM900/1800 Mobile Phone Models Using FDTD Method, *World Academy of Science, Engineering and Technology*, 3(1), pp.830-835.
- Al-Mously, S.I. and Abousetta, M.M., 2009b. *Cell Phones: The EM coupling with human body*, 1st ed. VDM Publishing House Ltd., ISBN: 978-3-639-21871-8.
- Anzaldi, G., Silva, F., Fernandez, M., Quilez, M., Riu, P.J., 2007. Initial analysis of SAR from a cell phone inside a vehicle by numerical computation. *IEEE Transactions on Biomedical Engineering*, 54(5), pp.921-930.
- Balanis, A., 1997. *Antenna theory: Analysis and design*, John Wiley and Sons.
- Beard, B., Kainz, W., Onishi, T., Iyama, T., Watanabe, S., Fujiwara, O., Wang, J., Bit-Babik, G. Faraone, A., Wiart, J., Christ, A., Kuster, N., Lee, A., Kroeze, H., Siegbahn, M., Keshvari, J., Abrishamkar, H., Simon, W., Manteuffel, D., Nikoloski, N., 2006. Comparisons of computed mobile phone induced SAR in the SAM phantom to that in anatomically correct models of the human head, *IEEE Transaction on Electromagnetic Compatibility*, 48(2), pp.397-407.
- Chavannes, N., Futter, P., Tay, R., Pokovic, K., Kuster, N., 2006. Reliable prediction of mobile phone performance for different daily usage patterns using the FDTD method. In: IEEE, *The international workshop on antenna technology (IWAT 2006)*. White Plains, NY, USA.
- Chen, Z.N., 2007. *Antennas for portable devices*, John Wiley & Sons, Ltd, Chichester.
- Diao, Y., Sun, W.N., Hung Chan, K.H., Leung, S.W., Siu, Y.M., 2013. SAR evaluation for multiple wireless communication devices inside a vehicle. In: *URSI, The international symposium on electromagnetic theory (EMTS)*, 20-24 May 2013. Hiroshima, Japan.
- Dimbylow, P.J. and Gandhi, O.P., 1991. Finite-difference time-domain calculations of SAR in a realistic heterogeneous model of the head for plane-wave exposure from 600MHz to 3GHz, *Physics in Medicine and Biology*, (6), pp.1075-1089.
- Dimbylow, P.J., and S. M. Mann, S.M., 1994. SAR calculations in an anatomically realistic model of the head for mobile communication transceivers at 900 MHz and 1.8 GHz, *Phys. Med. Biol.*, (39), pp.1537-1553.
- Ferrari, 2014. Overview; Ferrari Spider F430. [online] Available at: <http://auto.ferrari.com/en_EN/sports-cars-models/past-models/f430-spider/> [Accessed 25 June 2014].
- Francavilla, M., Schiavoni, A., Bertotto, P., Richiardi, G., 2001. Effect of the hand on cellular phone radiation, *IEE Proceeding of Microwaves, Antennas and Propagation*, 148, pp.247-253.
- Futter, P., Chavannes, N., Tay, R., et al., 2008. Reliable prediction of mobile phone performance for realistic in-use conditions using the FDTD method, *IEEE Antennas and Propagation Magazine*, 50(1), pp. 87-96.
- Gandhi, O.P., Lazzi, G., Furse, C.M., 1996. Electromagnetic absorption in the human head and neck for mobile telephones at 835 and 1900 MHz. *IEEE Transaction on Microwave Theory and Techniques*, 44(10), pp.1884,1897.
- IEC Standard, 2005, *62209-1 Human exposure to radio frequency fields from hand-held and body-mounted wireless communication devices—human models, instrumentation, and procedures—part 1: Procedure to determine the specific absorption rate (SAR) for hand-held devices used in close proximity to the ear (frequency range of 300 MHz to 3 GHz)*.
- IEEE Standard, 2003. *1528-2003 Recommended practice for determining the peak spatial-average specific absorption rate (SAR) in the human head from wireless communications devices: measurement techniques*.
- IEEE Standard, *1529 Recommended practice for determining the peak spatial-average specific absorption rate (SAR) associated with the use of wireless handsets—computational techniques*, draft standard.
- Jensen, M.A., Rahmat-Samii, Y., 1995. EM interaction of handset antennas and a human in personal communications. *Proceeding of the IEEE*, 83(1), pp.7-17.
- Kouveliotis, N.K., Panagiotou, S.C., Varlamos, P.K. and Capsalis, C.N., 2006. Theoretical Approach of the Interaction Between a Human Head Model and a Mobile Handset Helical Antenna Using Numerical Methods, *Progress In Electromagnetics Research, PIER 65*, pp.309-327.
- Lindberg, P., 2007. Wideband active and passive antenna solutions for handheld terminals, Ph. D. Uppsala University.
- Pedersen, G.F., 2012. Limit values for downlink mobile telephony in Denmark. Aalborg University. [pdf] Aalborg University. http://vbn.aau.dk/files/75767053/Limit_values_for_Downlink_Mobile_Telephony_in_Denmark.pdf [Accessed 20 May 2014].

Poole, I., 2004. Radio-Electronics.com; resources and analysis of electronics engineers. [online] Available at: <http://www.radio-electronics.com/info/cellular/telecomms/gsm_technical/power-control-classes-amplifier.php> [Accessed 20 May 2014].

Ruddle, AR., 2007. Computed SAR distributions for the occupants of a car with a 400 MHz transmitter on the rear seat. In: EMCZUR, *18th International Zurich symposium on electromagnetic compatibility*, September 2007. Munich, Germany.

Ruddle, AR., 2009. Computed SAR levels in vehicle occupants due to on-board transmissions at 900 MHz. In: *Antennas & propagation conference*, 16-17 November 2009. Loughborough, UK.

SEMCAD-X, 2009. Version 14.0 Altesch. Reference Manual, Simulation Platform for Electromagnetic Compatibility, Antenna Design and Dosimetry, SPEAG - Schmid & Partner Engineering AG: <<http://www.semcad.com>>.

Toftgard, J., Hornsleth, S.N. and Andersen, J.B., 1993. Effects on portable antennas of the presence of a person, *IEEE Transaction on Antennas and Propagation*, 41(6), pp.739–746.

Wang, J. and Fujiwara, O., 2003, Comparison and evaluation of electromagnetic absorption characteristics in realistic human head models of adult and children for 900-MHz mobile telephones. *IEEE Transaction on Microwave Theory and Techniques*, 51(3), pp.966-971.

Watanabe, S.-I., Taki, M., Nojima, T., Fujiwara, O., 1996. Characteristics of the SAR distributions in a head exposed to electromagnetic field radiated by a hand-held portable radio. *IEEE Transaction on Microwave Theory and Techniques*, 44(10), pp.1874–1883.

Yee, K.S., 1966. Numerical Solution of Initial Boundary Value Problems Involving Maxwell's Equations in Isotropic Media. *IEEE Transaction on Antennas and Propagation*, 14(3), pp.302-307.

The Effect of Substrate Temperature on the Structural Properties of Spray Pyrolysed Lead Sulphide (PbS) Thin Films

Mohammad G. Faraj¹ and Halo D. Omar²

^{1,2}Department of Physics, Faculty of Science and Health, Koya University
University Park, Danielle Mitterrand Boulevard, Koya KOY45, Kurdistan Region of F.R. Iraq

Abstract—Lead sulphide (PbS) films were prepared by the chemical spray pyrolysis technique using a solution of Lead nitrate and thiourea. PbS films were deposited (prepared) on glass substrate at varied temperature (250-350 °C). Effects of substrate temperature on the structural characteristics of the films were studied. The X-ray diffraction patterns' results reveal that the all of PbS films have a face centered cubic structure. The X-ray diffraction study showed that irrespective of substrate temperature all the films exhibits a preferred orientation along the (200) plane. The degree of preferred orientation increased with the substrate temperature. It was observed that the increase of the substrate temperature increase the diffraction peak intensity of (200) plane which resulted in increase in grain size and good crystallinity of the films.

Index Terms—Lead sulphide, chemical spray pyrolysis, thin film, semiconductor.

I. INTRODUCTION

PbS is a IV-VI compound semiconductor has a cubic lattice with unit cell face center cube (Lui and Zhang, 2000; Seghaier, et al., 2006), as shown in Fig.1.

Due to their direct narrow gap properties of PbS thin films regarded as a promising candidate for infrared detection for solar-control coatings (Thiagarajan, Beevi and Ramesh 2012; Choudhury and Sarma, 2009). Thin films of PbS have been prepared with various physical and chemical thin film deposition techniques, such as chemical bath deposition (Raniero, et al., 2012), physical vapor deposition (Mohammed, et al., 2012) and spray deposition (Anusuya, et al., 2012). Among these different techniques, spray technique

is advantageous on account of the low cost and its suitability for forming large area thin films (Ashour, Afifi and Mahmoud 1995).

In this paper, PbS thin films deposited on glass substrate by chemical spray pyrolysis at different substrate temperatures (250, 300 and 350 °C). The influence of substrate temperature on the structural properties of the PbS thin films was observed and the results are reported.

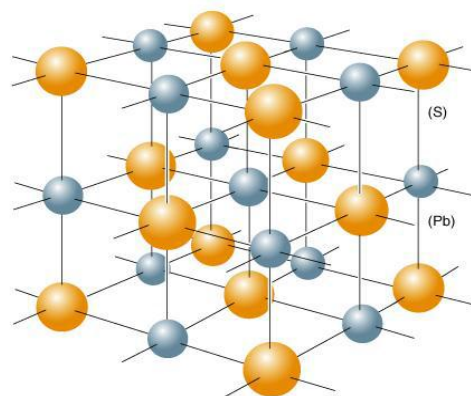


Fig.1. Crystal structure of PbS, adapted from Sze and Ng, (2007).

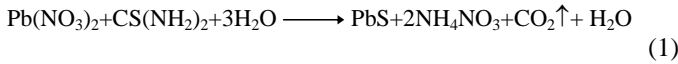
II. EXPERIMENTAL DETAILS

The glass substrates were washed with alcohol and then ultrasonically cleaned in alcohol for 10 minutes. Later, deionized water was used to rinse the substrate. Lastly, dried with nitrogen gas.

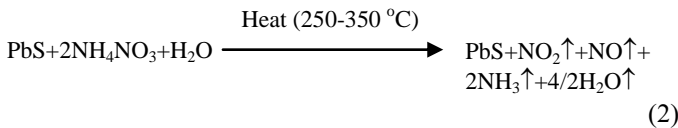
Before starting the deposition, the solutions are mixed according to the film components (after found their weight by this equation ($W=M \times M.wt \times V/1000$, where M is the molarity, M.wt is the molecular weight and V is the volume) by solving the salts in the distilled water as follows:

- Thiourea solution [$CS(NH_2)_2$]: This solution was prepared with molarities (0.1 M), from solving (0.761 gm) of thiourea in (100 ml) of distilled water.
- Lead Nitrate solution [$Pb(NO_3)_2$]: This solution was prepared with molarities (0.1M), from solving (2.78 gm) of lead acetate in (100 ml) of distilled water.

After getting the different amount of solutions according to the required ratio and volume, the prepared solution was put on magnetic stirrer about 10 minutes to be sure the solutions have been mixed properly. Then the solution of Lead Nitrate and Thiourea are mixed to obtain the PbS and ammonium nitrate according to the reaction equation:



The resulting solution was deposited on glass substrate at different temperature (250, 300 and 350 °C), and the ammonium nitrate dissolved by heating as seen in the reaction equation (Ibrahim, 2012).



PbS films were deposited on glass substrate by chemical spray pyrolysis technique. The description of the experimental set-up of chemical spray pyrolysis (CSP) system is presented in Fig. 2. PbS films were prepared by spraying an aqueous solution of Lead Nitrate and Thiourea on hot glass substrates at different temperature (250, 300 and 350 °C). The carrier gas used for spraying was compressed air. The thickness of the film was optimized to be 500 nm. The film thickness was measured by the weighting method via a digital balance type (Meter AE-160) with sensitivity of 10^{-4} gm, and the thickness was calculated according to the following equation (Faraj and Ismail, 2009):

$$t = \frac{\Delta m}{\rho \cdot A} \quad (3)$$

where, t is the thickness of the film, Δm : is the mass of the film, ρ is the total density of the film and A is the area of the film.

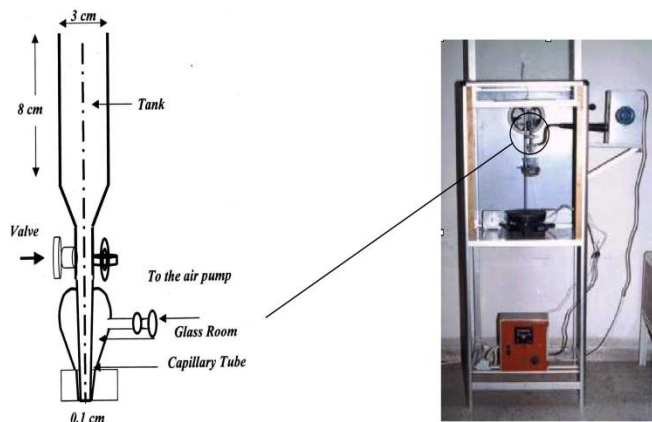


Fig. 2. Experimental set-up of spraying apparatus (right), and layout of enlarged spraying glass nozzle (left).

The crystallographic structure of the prepared PbS thin films was determined using a high resolution x-ray diffractometer

system (model: panalytical empyrean) with $\text{CuK}\alpha$ radiation (λ) of 0.154 nm at the department of Physics, Koya University.

III. RESULTS AND DISCUSSION

Fig. 3 shows the typical XRD pattern of the PbS samples for three different substrate temperatures. All PbS films have face centered cubic structure as confirmed by standard ASTM data (Masumoto, et al., 1992). XRD patterns of all the PbS thin films showed sharp [111] and [200] peaks along with minor peaks of [220], [311], [222], [420], [422] and [511] planes corresponding the face centered cubic structure of PbS thin films. These XRD results confirm the proper phase formation of the PbS films.

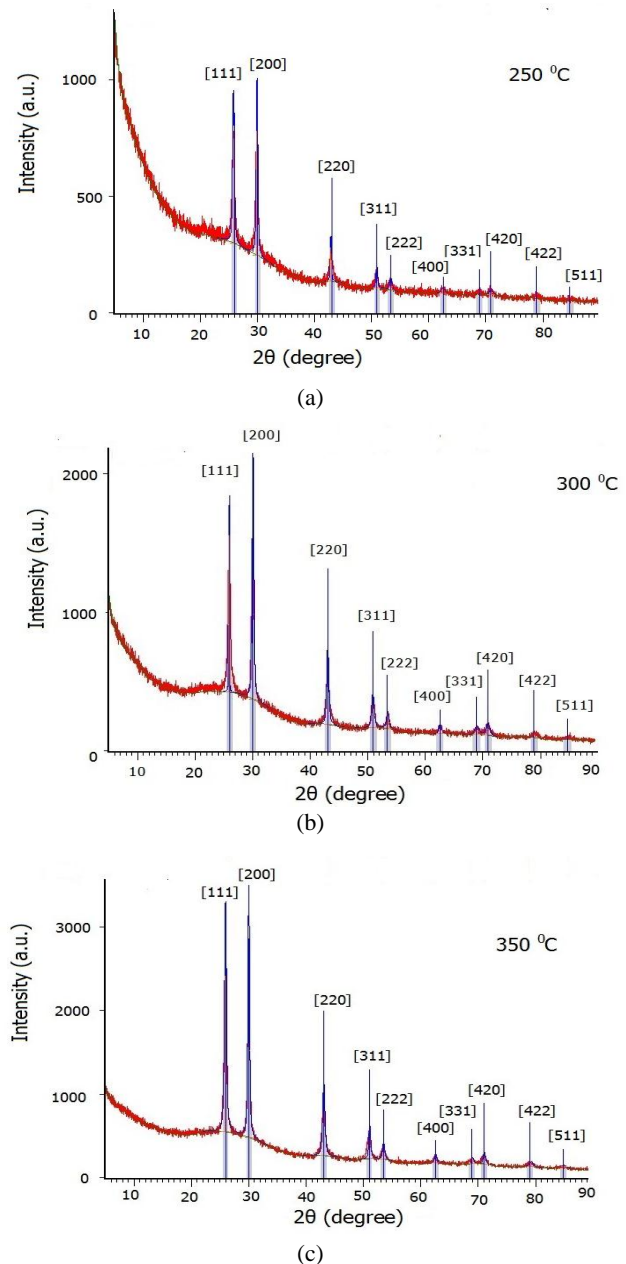


Fig. 3. XRD patterns of PbS films at substrate temperatures of; (a) 250 °C, (b) 300 °C and (c) 350 °C.

XRD patterns shows a clear dependent of the peaks intensity on the substrate temperature of the deposited films and suggests that the deposited PbS films are crystalline which is similar to reported in the literature (Rajashree, et al., 2014; Abbas and Jafir, 2012). The crystalline grain size (t) of the PbS films was determined with the Scherrer formula (Birks, 1946).

$$t = \frac{0.9\lambda}{\beta \cos\theta} \quad (4)$$

where, β is the full width at half maximum (FWHM) of the peak, λ is the wavelength of the X-ray, 1.5406 Å, and θ is the peak position. Based on the line width of the (200) diffraction peak, the crystalline grain size for the PbS films with differing substrate temperature shown in Fig. 4, and the grain size increase with increasing substrate temperature especially at 350 °C (Ibrahim, et al., 2012).

For studied films the preferential orientation value of (200) plane has the highest value compared to other planes. The obtained result indicates a strong orientation growth along the (200) plane which is agreed with that reported by (Seghaier, et al., 2006). The variation in preferential orientation factor $f(hkl)$ for (200) as a function of substrate temperature shown in Fig. 5. The maximum peak value at 350 °C indicate the better crystallinity of the deposited PbS (Ibrahim, et al., 2012; Abbas and Jafir, 2012; Rajashree, et al., 2014).

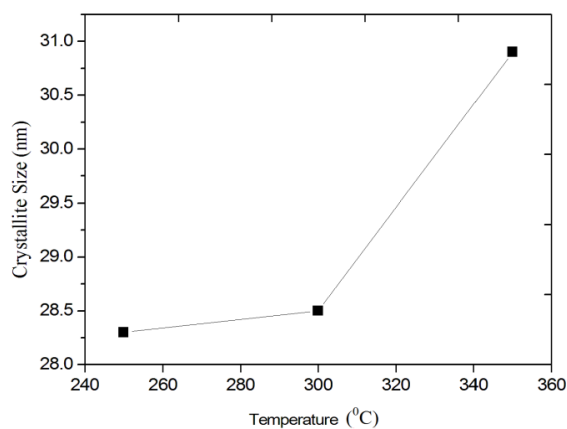


Fig. 4. Crystalline grain sizes as a function of substrate temperatures.

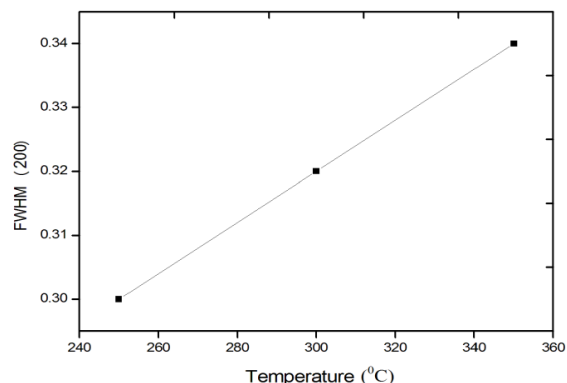


Fig. 5. Variation of FWHM of preferential orientation (200) of PbS films with substrate temperature.

IV. CONCLUSION

Lead sulphide (PbS) thin films were deposited on glass substrates with chemical spray pyrolysis. Effects of substrate temperature (250, 300 and 350 °C) on the structural characteristics of the films deposited were studied. X-ray diffraction patterns confirm the proper phase formation of the PbS. For studied films the preferential orientation value of (200) plane has the highest value compared to the planes. The grain size of the PbS films increased with increasing temperature. The values of crystallite size are temperature dependent were found to be in the range of 28.3 – 31 nm. The films were fabricated at the lowest temperature have the least crystalline quality as was observed in XRD patterns. The higher the substrate temperature the better crystallinity was observed.

REFERENCES

- Abbas, T.A. and Jafar, A.O., 2012. The effect of substrate temperature on the physical properties of spray pyrolysed CdS thin films. *Journal of Education and Science*, 25(4), pp.77-85.
- Anusuya, M., Saravanan, V., Ramesh, T., and Beevi M.M., 2013. Physical Properties of spray pyrolytically LI doped Pbs thin films. *Journal of Non-Oxide Glasses*, 5(1), pp.33-37.
- Ashour, A., Afifi, H. and Mahmoud, S.A., 1995. Structural study of ZnS thin films prepared by spray pyrolysis. *Thin Solid Films*, 263(2), pp.248-251.
- Birks, L., 1946. Particle size determination from X-Ray Line Broadening. *Journal of Applied Physics*, 17(8), pp.687-692.
- Choudhury, N. and Sarma, B., 2009. Structural characterization of lead sulfide thin films by means of X-ray line profile analysis. *Bulletin of Materials Science*, 32(1), pp.43-47.
- Ibrahim, A.E., 2012. Effect of doping by copper on the optical properties on the films prepared by thermal chemical spray. *Tikrit Journal of Pure Science*, 17(1), pp.215-220.
- Ibrahim, A.M., Ismail, R.A. and Ali, A.Y., 2012. Effect of Substrate Temperature on the structural surface morphological and optical properties of nanostructured CdS thin films. *Tikrit Journal of Pure Science*, 17(2), pp.151-155.
- Ismail, R.A. and Faraj, M.G., 2009. Study of optical&electrical properties of CdO prepared by chemical spray pyrolysis, *Journal of College of Education, AL- Mustansiriyah University*, 3(1), pp.532-539.
- Lu, X. and Zhang, M., 2000. Studies on PbS and PbSe detectors for IR system. *International Journal of Infrared and MillimeterWaves*, 21(10), pp.1697-1701.
- Mohammed, A.J., Salim, S.R., Jaleel, M.S. and Hassan, M.A., 2012. Structural Characterization of Lead Sulfide Thin Films by means of FTIR Analysis after Irradiation of β -ray. *British Journal of Science*, 7(1), pp.35-37.
- Masumoto, K., Mochizuki, K., Abe, S., 1992. Solubility range and lattice constant of new quaternary solid solution semiconductor $Pb_{1-x}Ca_xS_{1-y}Se_y$ for mid-infrared lasers. *Journal of the Japan Institution of Metals*, 56, pp.1479 – 1484.
- Rajashree, C., Balu, A.R. and Nagarethinam, V.S., 2014. Substrate temperature effect on the physical properties of spray deposited Lead sulfide thin films suitable for solar control coatings. *International Journal of ChemTech Research*. 6(1), pp.347-360.
- Raniero, L., Ferreira, C.L., Cruz, L.R., Pinto, A.L. and Alves, R.M.P., 2010. Photoconductivity activation in PbS thin films grown at room temperature by

chemical bath deposition. *Physica B: Condensed Matter*, 405(5), pp.1283-1286.

Seghaier, S., Kamoun, N., Brini, R. and Amara, A.B., 2006. Structural and optical properties of PbS thin films deposited by chemical bath deposition. *Materials Chemistry and Physics*. 97, pp.71-80.

Sze, S.M. And Ng, K.K. 2007. *Physics of semiconductor devices*. New Jersey: John Wiley and Sons.

Thiagarajan, R., Beevi, M.M. and Ramesh, T., 2012. Influence of reactant concentration on nanocrystalline PbS thin films prepared by Chemical Spray Pyrolysis. *Optoelectronics and Advanced Materials – Rapid Communications*, 6(1-2), pp.132-135.

Investigations of Flare Gas Emissions in Taq Taq Oil Field on the Surrounding Land

Jafar A. Ali¹ and Loghman A. Khodakarami²

^{1,2}Department of Petroleum Engineering, Faculty of Engineering, Koya University
University Park, Danielle Mitterrand Boulevard, Koya KOY45, Kurdistan Region of F.R. Iraq

Abstract—Environmental pollution caused by oil takes many different forms; one of the most damaging sources is simply the combustion of oil products, such as a well flare burn-off. This paper presents the results of a survey of the agriculture lands around the Taq Taq Oil Production Company. The aim of the survey was to determine the potential contamination caused by the gas emissions from the well flares. Taq Taq field is located in the Kurdistan Region of Iraq, 60 km north of the giant Kirkuk oil field, 85 km south-east of Erbil and 120 km north-west of Suleimani. Samples of soil were collected from several locations around the site and analyzed to determine the content of Polycyclic Aromatic Hydrocarbons PAH present. A gas chromatography linked to a mass spectrometry (GCMS) machine was used for these measurements. The PAH contamination at each location of soil was determined and the 16-PAHs, as listed in the US Environmental Protection Agency (EPA) documentation were investigated. The average content of total PAH in all samples of the agricultural soil was $0.654 \text{ mg}\cdot\text{kg}^{-1}$ with the concentrations ranging from 0.310 to $0.869 \text{ mg}\cdot\text{kg}^{-1}$. It was found that the PAH concentrations decreased with increasing distance from the TTOPCO oil field, indicating that pollution was evident, the area close to the field being more affected by the gas pollution.

Index Terms—Flare, geographic information system, pollution, polycyclic aromatic hydrocarbon, TTOPCO.

I. INTRODUCTION

The concern for oil field emissions of pollutants and their effect on the Kurdistan environment has been increasing since 2004 and in Koya city since 2005 when Taq Taq field started to expand by Addax Petroleum world Class Company. Excessive discharge of hydrocarbons to flare is resulting in

flooding of black smoke (plume) which is caused a disaster to the environment.

Soil is the primary environmental reservoir for persistent organic pollutants (POPs) in the terrestrial environment. Once deposited, POPs may reside in the soil for many years. However, soil may not be a permanent sink for these compounds; they tend to recycle continuously between the atmosphere and the terrestrial environment over long periods of time. The soil therefore can either be a sink for POPs or become a source of POPs back into the atmosphere (Mackay, 2001; Cousins, Beck and Jones, 1999). Among the persistent organic pollutants, polycyclic aromatic hydrocarbons (PAHs) are very important. Polycyclic aromatic hydrocarbons (PAHs) contain complex chemicals which include carbon and hydrogen with a fused ring structure, containing at least two benzene rings (Sexton, et al., 2011). PAHs are generally produced by the incomplete combustion of organic material, for example, fossil fuels. Burning carboniferous materials release copious amounts of smoke containing polynuclear aromatic hydrocarbons (PAHs). Via atmospheric deposition PAHs also reach soil and sediments in areas remote from industry, airports and highways. In addition, oil spills due to accidents or careless oil handling are polluting factors. More than 100 PAHs have been characterized in nature, sixteen of which were classified as priority pollutants according to US Environment Protection Agency (Bishnoi, et al., 2005). PAHs that have accumulated in soils may directly or indirectly pose a risk to human and ecosystem health (Jones, 1991).

Polynuclear aromatic hydrocarbons have been documented to cause several health problems (Hati, et al., 2009). Some PAHs and their derivations are highly toxic. Their mutagenic or carcinogenic properties are the main risk to human health (Prycek, Ciganek and Srinek, 2007). Risk assessment and source apportionment of PAH-contaminated soils require accurate analysis of the concentration of each PAH component in the soil. At present the analytical equipment used for the measurement of PAHs in soils mainly comprises gas chromatography (GC) (Kuosmanen, et al., 2003; Zuazagoitia, Millán, and Garcia-Arrona, 2009), gas chromatography–mass spectrometry (GC–MS) (Ene, et al., 2012) and high performance liquid chromatography (HPLC) (Yang, et al., 2011). In this study all samples were analyzed by gas chromatography–mass spectrometry. Soil contamination by

refining oil products has been studied widely by the researchers across the world. Since the beginning of the last century the oil industries are running in Iraq, whilst in Kurdistan Region the oil industries started after Kurdish uprising in 1991. Although the large number of oil fields across the country, the researchers have not studied fairly their effects on the environment.

The objective of this paper is to investigate the occurrence of PAHs in agricultural soils that are directly impacted by Taq Taq oil field in topsoil in the vicinity of a TTOPCO (5000-meter buffer) in the Kurdistan region, This information on PAH distribution can be used for health risk assessment and future urban development.

II. METHODS AND MATERIALS

A. Study Site

The area of the study site is about 2827.4 Hectares (ha) and located between 453636 and 459635 longitudes and 3981823 and 3987823 latitudes. The Taq Taq is one of the largest oil fields in Kurdistan Region, it is located near the town of Koya in the heart of the region; 60 km north of the giant Kirkuk oil field, 85 km south-east of Erbil and 120 km north-west of Suleimani, Fig. 1. Addax Petroleum was the first international oil company participated to develop Taq Taq field in 2005 (Sinopic, 2013). Taq Taq is currently producing 40000 bpd of oil and burning the waste gases via two flares, one of them is not burning the gases properly so it is discharging wastes more than the other. The predominant land use of these catchment areas are: agriculture with predominant crops of wheat, barley, alfalfa and potato, garden and orchard. The minimum and maximum height of study area from sea surface is 449 m and 639 m respectively.

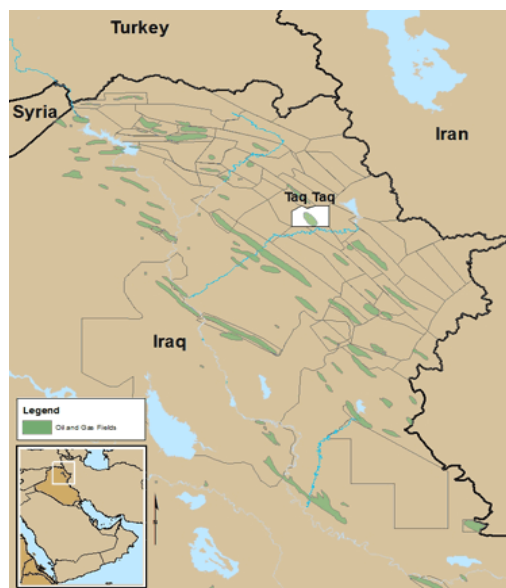


Fig. 1. The field location, from Addax Petroleum Website.

B. Sampling of Soils and Analytical Methods

Soil Sampling and Preparations

Twelve composite soil samples were collected from 0-10 cm depth by dividing the affected area into a grid of 500 m \times 500 m using random systematic method, Fig. 2. The area at each sampling point was about 20 m \times 20 m grid and soil samples were taken from each corners and center of each grid. The sampling sites were selected in order to reflect the diverse exposure of soils to the pollution sources and dominant wind directions. The sampling sites are shown in Fig. 2 and described in Table 1. The samples were collected from the surface layer (from 0-10 cm depth), after removing grass in agricultural soil.

Approximately 500 g of material were collected from a square area of 20 \times 20 m in each sampling site. All samples were put into envelope of sealed aluminum foil containers with a minimum headspace of air, and immediately transported to the laboratory. The envelopes of the samples were kept with ice through the survey and during the transportations to avoid the escaping of hydrocarbons, in laboratory they are kept in refrigerator. The containers were used only once with clean equipment for each sample.

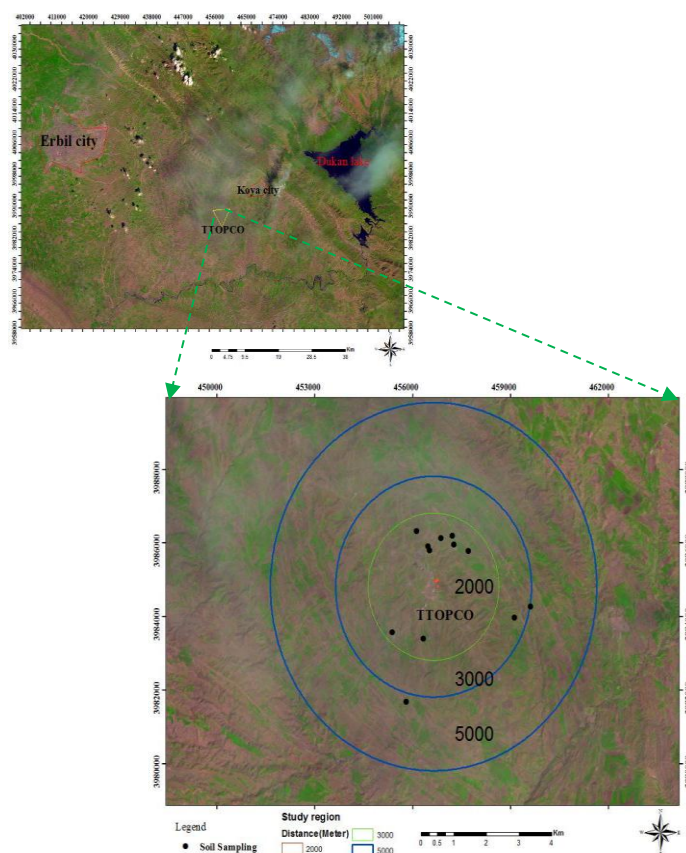


Fig. 2. The status of study region and samples stations.

TABLE I
PAH CONCENTRATIONS IN THE SOIL SAMPLES AT TTOPCO (5000-METER BUFFER), (mg·kg⁻¹)

Station	NAP	ANY	FLU	PHEN	ANT	FLT	PYR	BaA	CHR	BbF	BkF	BaP	IPY	DBA	BgP	ACP	tPAHs
1	0.060	ND	0.053	0.060	0.061	0.070	0.052	ND	0.080	0.060	0.059	0.056	ND	ND	0.060	ND	0.671
2	0.070	0.052	0.060	0.069	0.058	0.067	0.08	0.056	0.082	0.063	0.090	0.051	ND	ND	0.055	ND	0.853
3	0.065	ND	0.055	0.058	0.070	0.077	0.075	0.064	0.076	0.070	0.089	0.053	0.060	ND	0.057	ND	0.869
4	0.055	0.051	0.051	0.067	0.087	0.058	0.069	ND	0.077	0.075	0.078	0.065	0.064	ND	ND	ND	0.797
5	0.075	ND	ND	0.059	0.076	0.053	0.070	0.076	0.065	0.066	0.092	ND	ND	ND	ND	ND	0.632
6	0.080	ND	ND	0.073	0.069	0.087	0.078	0.063	ND	ND	0.078	ND	0.070	ND	0.059	ND	0.657
7	0.081	ND	ND	0.090	0.083	0.065	ND	ND	ND	0.077	0.087	0.065	ND	ND	ND	ND	0.548
8	0.056	0.054	ND	0.088	0.055	ND	ND	0.051	0.078	0.065	0.065	ND	ND	ND	ND	ND	0.512
9	0.057	ND	ND	ND	0.058	ND	ND	0.053	0.077	ND	0.065	ND	ND	ND	ND	ND	0.310
10	0.052	ND	0.053	ND	0.051	0.051	0.054	ND	ND	0.067	0.073	0.065	ND	ND	ND	ND	0.466
11	0.055	ND	ND	0.087	0.052	ND	0.056	0.063	0.090	0.077	0.079	0.073	0.080	ND	0.060	ND	0.772
12	0.063	0.053	0.053	0.098	0.074	0.090	ND	0.055	0.079	ND	0.080	ND	0.063	ND	0.055	ND	0.763

ND = Not Detected, tPAHs = Total PAHs

Extraction and Analysis of PAHs

Initially, all samples were thoroughly homogenized by a sieve shaker on a 2 mm metal sieve. The water content (10-14% w) was determined on portions of homogenized samples after 24h drying at 105 °C. Different drying procedures, including thermal and chemical drying, were applied. Thermal drying was performed at 40 °C for five days and at 105 °C for 24h. The soil samples were subsequently extracted using the Ultrasonic Extraction method. Four gram from each soil samples were subjected to ultrasonic extraction according to the analytical scheme described by Berset, et al. (1999). Briefly, the samples were put into glass conic bottles with 25ml of a solvent mixture (hexane/acetone 85/15 v/v) and were left in the ultrasonic bath (300 W) for 30 min. The extracts were filtered twice through Whatman paper No 42 (2.5 µm pore size) and stored in the refrigerator in dark amber glass flasks, closed with teflon screw caps for subsequent analysis. A known amount of internal standard (hexamethylbenzene) was added to all extracts prior to PAHs analysis. These PAHs were quantitatively analyzed by GCMS (GC17AAF) using a 30 m × 0.25 mm fused silica capillary column (SUPELCO PTE) with helium as the carrier gas at flow rate of 1.2 ml·min⁻¹. 1 µL of aliquot from a known volume of analytic solution was injected manually. Verification of peaks was carried out based on key fragment ions, retention times compared to those of external PAHs standards, and/or mass spectra. Only those peaks located within the proper range (2%) of retention time were integrated for qualification and quantification. Quantitation were performed using external standards of a mixture of PAHs.

The GC temperature program was as follows: initially at 80 °C for 5 min, increased to 290 °C at 3 °C/min, and held for 30 min. A 1 µL sample was injected into the split/split less injector with a 5 min solvent delay.

All solvents used in this study were of analytical grade from Merck. A standard mixture of the 16 EPA priority PAHs, 2000 µg/ml each from Supelco was used for the GC-MS calibration and n-dodecane (99%) from Aldrich as internal standard. Aluminum oxide (90 active neutral), 70-230 mesh from Merck and Silica gel, 100-200 mesh from Aldrich, were also used. In this study, 16 priority pollutant PAHs identified by the US Environmental Protection Agency (EPA) were analyzed.

Sixteen USEPA (United State Environmental Protection Agency) priority PAHs were selected and they are abbreviated as Naphthalene (NAP), Acenaphthylene (ANY), Acenaphthene (ACP), Fluoranthene (FLU), Phenanthrene (PHEN), Anthracene (ANT), Fluoranthene (FLT), Pyrene (PYR), Benz(a)anthracene (BaA), Chrysene (CHR), Benzo(b)fluoranthene (BbF), Benzo(k)fluoranthene (BkF), Benzo(a)pyrene (BaP), Indeno(1,2,3-cd)pyrene (IPY), Dibenz(a,h)anthracene (DBA), Benzo(g,h,i)perylene (BgP).

C. GIS Mapping

A geographic information system (GIS) was used to create a survey map of PAH. A GPS receiver of type (GPS Garmin 62s, USA) was used to record the position of sample locations. From the Global Positioning Satellite (GPS) receiver, the WG84 coordination system was transformed to the TM coordination system to fit the actual map. For the distribution map, GIS software, Arc GIS (ver. 10.1, ESRI, USA), was used, and the concentration of PAH was displayed as distribution map on the GIS map.

III. RESULTS AND DISCUSSION

Most PAHs reach the soil via deposition from the atmosphere, and PAH concentrations in the soils tend to increase with the increasing impact of industry, traffic, and domestic heating (Jones, et al. 1989). It is known that low molecular weight PAHs are relatively more volatile and could likely be evaporated by the high temperature and solar radiation of tropical soils.

The measured data for every individual and total PAHs are presented in Table 1, there are PAHs have not been detected at some locations, but Acenaphthene and Dibenz(a,h)anthracene were totally not detected in all samples. The range and arithmetic mean and median of PAH concentrations in soil samples are presented in Table 2. Total PAH concentrations ranged from 0.310 to 0.869 mg·kg⁻¹ dry weight, with an average value of 0.654 mg·kg⁻¹. It is clear from the presented tables that the measured detected values of PAHs are close to zero or they are the minimum. Whilst the black plume that is released from Taq Taq field indicate to more than these values of PAHs could be found in the surrounding lands. The reason of that is due to lack of facilities that were between hands during this research work.

TABLE II
MEAN, MEDIAN AND RANGE OF PAH IN COLLECTED SOIL SAMPLES (mg·kg⁻¹)

	Mean	Median	Range
Naphthalene	0.064	0.0615	0.052 - 0.081
Acenaphthylene	0.042	0.0520	0.000 - 0.054
Fluorine	0.054	0.0530	0.051 - 0.060
Phenanthrene	0.075	0.0710	0.058 - 0.098
Anthracene	0.066	0.0650	0.051 - 0.087
Fluoranthene	0.069	0.0670	0.051 - 0.090
Pyrene	0.067	0.0695	0.052 - 0.080
Benz(a)anthracene	0.053	0.0560	0.000 - 0.076
Chrysene	0.078	0.0780	0.065 - 0.090
Benzo(b)fluoranthene	0.069	0.0670	0.063 - 0.077
Benzo(k)fluoranthene	0.078	0.0785	0.059 - 0.092
Benzo(a)pyrene	0.061	0.0650	0.051 - 0.073
Indeno(1,2,3-cd)pyrene	0.056	0.0635	0.000 - 0.080
Dibenz(a,h)anthracene	0.000	0.0000	ND
Benzo(g,h,i)perylene	0.058	0.0580	0.055 - 0.060
Acenaphthene	0.000	0.0000	ND
tPAHs	0.654	0.6640	0.310 - 0.869

Fig. 3 presents the total PAHs profile at all locations, at location 3 the total PAH was detected as maximum, whilst the minimum value was detected at location 9. In Fig. 4, the two dimensional map of PAH distribution around the survey area is presented, the red color indicates to highest polluted area and the blue color is the area that is less affected.

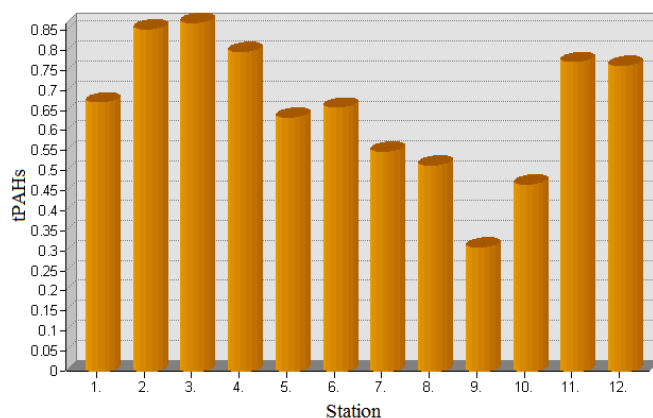


Fig. 3. Total PAH profile at all stations.

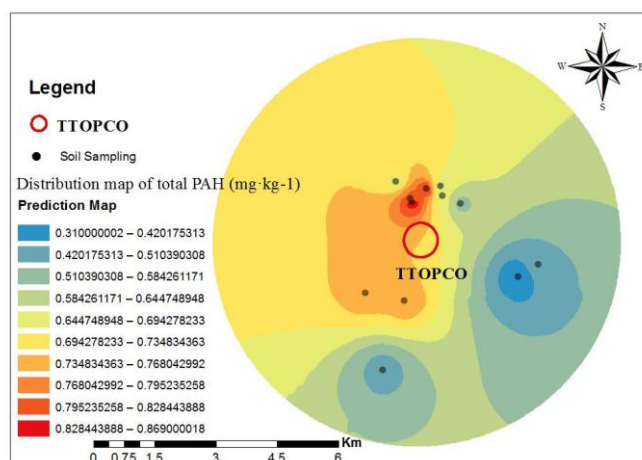


Fig. 4. Total PAH distribution for the surveyed area.

IV. CONCLUSION

The highest concentration of total identified PAHs was obtained at station 3 with the concentration of 0.869 mg·kg⁻¹ and the lowest were detected at stations 9 and 10 with values of 0.310 and 0.466 mg·kg⁻¹ respectively. Evaluation of several diagnostic ratios suggests that these PAHs were mainly derived from combustion of the flare rather than petro-genic. Stations that have more PAHs detected are located to the north west of the field where the direction of the wind most of times. The detected PAHs in this study are less than that is expected; this is because of lack of facilities. It is necessary to obtain correct and adequate emission inventory to minimize the impact of pollutants discharged from flare. Therefore, in future this work should be repeated using closer laboratories for testing the samples to avoid the possibility of hydrocarbons escape and achieving better results.

REFERENCES

Bishnoi, N.R., Mehta, U., Sain, U. and Pandit, G., 2005. Quantification of polycyclic aromatic hydrocarbons in tea and coffee samples of Mumbai city using high performance liquid chromatography. *Environ. Monit. Assess.*, 107(1-3), pp.399-406.

- Berset, J.D., Ejem, M., Holzer, R. and Lischer, P., 1999. Comparison of different drying, extraction and detection techniques for the determination of priority polycyclic aromatic hydrocarbons in background contaminated soil samples. *Anal. Chim. Acta*, 383(3), pp.263-275.
- Cousins, I.T., Beck, A.J. and Jones, K.C., 1999. A review of the process involved in the exchange of semi-volatile organic compounds (SVOC) across the air-soil interface. *Science of the Total Environment*, 228(1), pp.5- 24.
- Ene, A., Bogdevich, O., Sion, A., Spanos, T., 2012. Determination of polycyclic aromatic hydrocarbons by gas chromatography–mass spectrometry in soils from southeastern Romania. *Microchem. J.* 100(1), pp.36–41.
- Hati, S.S., Dinar, G.A., Egwu, G.O. and Ogunbuaja, V.O., 2009. Polycyclic Aromatic Hydrocarbons (PAHs) contamination of synthetic industrial essentials utilized in the Northern Nigeria. *African Journal of Pure and Applied Chemistry*, 3(5), pp. 86 – 91.
- Jones, K.C., Stratford, J.A., Waterhouse, K.S., and Vogt, N.B., 1989. Organic contaminants in Welsh soils: Polycyclic aromatic hydrocarbons. *Environmental Science and Technology*, 23, pp.540–550.
- Jones, K.C., 1991. Contaminant trends in soils and crops. *Environ. Pollut.* 69(4), pp.311-325.
- Kuosmanen, K., Hyötyläinen, T., Hartonen, K., Riekkola, M.L., 2003. Analysis of polycyclic aromatic hydrocarbons in soil and sediment with on-line coupled pressurised hot water extraction, hollow fibre microporous membrane liquid– liquid extraction and gas chromatography. *Analyst*, 128(5), pp.434–439.
- Mackay, D., 2001. *Multimedia Environmental Models: the Fugacity Approach*, 2nd ed. Lewis/CRC, Boca Raton FL.
- Prycek J., Ciganek, M. and Srinek, Z., 2007. Clean up of extracts for nitrated derivatives of polycyclic aromatic hydrocarbons analysis prior their gas chromatography determination. *Journal of the Brazilian Chemical Society*, 18(6), doi:10.1590/S0103-50532007000600004.
- Sexton, K., Sahmas, J.J., MacDonald, T.J., Gowen, R.M.Z., Miller R.P., McCormick, J.B. and Fisher-Hosh, S.P., 2011. PAHs in Maternal Unbilical cord blood from pregnant Hispanic women living in Brownsville, Texas. *International Journal Environmental Research and Public Health*, 8(8), pp.3365 – 3379.
- Sinopec – Addax Petroleum Foundation – Middle East, 2013. [Online] Available at <https://www.addaxpetroleum.com/operations/middle-east>. [Accessed 25 July 2013].
- Yang, F., Long, Y.M., Shen, R., Chen, C.Y., Pan, D., Zhang, Q.L., Cai, Q.Y., Yao, S.Z., 2011. Ultrasonication extraction coupled with magnetic solid-phase clean-up for the determination of polycyclic aromatic hydrocarbons in soils by high-performance liquid chromatography. *J. Sep. Sci.* 34(6), pp.716–723.
- Zuazagoitia, D., Millán, E., Garcia-Arrona, R., 2009. Comparison of two extraction methods for the determination of polycyclic aromatic hydrocarbons in surface soils using headspace SPME with GC–FID. *J. Chromatogr. Sci.*, 47(2), pp.97–102.

Photon Dose Enhancement Ratio at the Transition Region of Dissimilar Media

Maan S. Al-Arif

Department of Physics, Faculty of Science and Health, Koya University
University Park, Danielle Mitterrand Boulevard, Koya KOY45, Kurdistan Region of F.R. Iraq

Abstract—Accurate measurement was carried out for the dose gradient in Teflon irradiated with filtered X-ray spectra having effective energies of 40 keV and 55 keV when in contact with aluminum, titanium, copper, and tin. At low photon energies, the interface region is only extended for about 10 microns from the interface, therefore, ultra-thin LiF/Teflon discs of the order of 3 microns thick was developed and used to measure directly the dose gradient in Teflon. Due to the relatively large slope of the depth dose curves near the interfaces, a displacement correction factor was introduced to determine the effective measuring point of the detector. A fitting exponential formula is suggested and used to estimate the dose gradient for Bone-Teflon interface. The interface dose for Bone-Teflon is 3.8 times the equilibrium dose at 70 KV, while it is about 3.1 at 100 KV.

Index Terms—Buildup dose, effective energy, radiation, transition region.

I. INTRODUCTION

Radiation dose distribution at interfaces region between dissimilar media are of wide interest in for example, the application of X-ray and gamma rays in the treatment where the presence of air cavity disturb the photon field in a region between tissue-air inside the lungs (Shiu and Hogstrom, 1991; Li XA and Holmes, 2000; Joshi, et al., 2010; Chandra, et al., 2010), in radiotherapy treatment of head and neck (Kinhikar, et al., 2014), in diagnostic radiology where tissue are in contact with high atomic number medium (Nicopoulou-Karayianni, et al., 2003), in radiological protection and nuclear shielding engineering problems, and in the induced of hard and soft errors in VLSI solid state circuitry (Das, et al., 2001). For biophysical application, the effects of low energy photon field are of special importance for several reasons:

- 1- The biophysical effectiveness of secondary electrons reaches a maximum at energies between 250 eV and 50 keV.
- 2- The dose in soft tissue near an interface with material of higher atomic number can exceed the equilibrium dose because of the contributions from back scattering and photoelectrons.
- 3- Attempts to correlate the sparse experimental data with theories had indicated the need for more detailed experimental information.

II. MATERIAL AND METHOD

Accurate measurements were made to assess the dose gradient in Teflon taken as a typical example of low atomic number material, in contact with aluminum, titanium, copper, and tin irradiated with filtered X-ray spectra having effective energies of 40 keV (70 KV) and 55 keV (100 KV). For simplicity, plane interface geometry was used in the measurements. Since the transition region extended only for a distance of about 10 microns from the interface, ultra-thin, 30% by weight, LiF/Teflon TLD of 3 micron thick was developed in our laboratory. The ultra-thin discs were first soft and difficult to handle. This problem was overcome by sandwiching the soft discs between two micro-slides glass in an oven at a temperature of 280 °C for two hours. The micro-discs become rigid and more easily to be handled by vacuum tweezers. The average weight of the discs determined immediately after cutting was 0.18 mg with accuracy not worse than ± 0.015 mg. Direct measurement of the disc thickness with a standard digital micrometer yield values of the order of 3 ± 0.5 microns. The thickness was also checked by a Mercer digital metric gauge unit type 122D. An average value of 3 ± 0.5 microns was assumed for all discs. Measurements of the dose gradient, the build-up factor, were carried-out by increasing the separation distance between the detector and the high atomic number media, see Fig. 1.

The radiation beam was directed perpendicularly to the surface of an approximately cylindrical phantom of Teflon plastic. The entrance field, symmetrically situated on the phantom surface, was 1.0 cm diameter defined by means of a special mask made of, lead, copper, aluminum, and Perspex (Al-Arif, 2013b). The mask was arranged so that the material nearest to the detector was the material with the lowest k-edge.

ARO, The Scientific Journal of Koya University
Volume II, No 2(2014), Article ID: ARO.10046, 04 pages
DOI: 10.14500/aro.10046
Received 14 June 2014; Accepted 04 November 2014
Regular research paper: Published 15 December 2014
Corresponding author's e-mail: maan.safa@koyauniversity.org
Copyright © 2014 Maan S. Al-Arif. This is an open access article distributed under the Creative Commons Attribution License

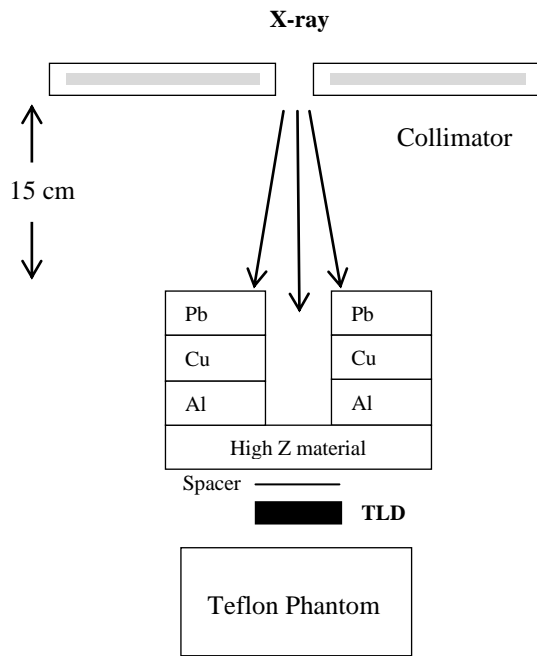


Fig.1. Experimental setup for dose gradient measurement.

The materials with progressively higher k-edges were mounted on the top of this. Thus, the incident spectrum progressively degenerated to negligible proportions in the graded absorber.

The ultra-thin discs were placed in between the high and the low atomic number media. In practice, it is desirable to know to what degree the dose to a low atomic number medium has been increased by the presence of higher atomic number medium. Thus rather than measure the absolute dose values, the dose build up ratio were determined. Each measurement for the dose gradient was repeated five times. The standard deviations of the mean were calculated, see Table I and Table II. The light outputs from the TLD detectors were normalized to unit weight and recorded as TL/mg. The thickness of each high atomic number material was chosen to be greater than the maximum electron range generated to ensure that the electronic equilibrium was established but sufficiently thin so that attenuation of the X-ray beam did not cause a significant quality change. The thicknesses chosen were 60, 50, 25, and 30 microns respectively. Due to the relative sharp dose gradient near to the interface, theoretical displacement correction factor were calculated and used to specify the effective measuring point of the 3 micron TLD discs at the transition region (Al-Arif, 2013a).

III. RESULTS AND DISCUSSION

Tables I and II show the displacement correction factor, the measured dose buildup ratio and the effective measuring point of the TLD's at the transition region for the two effective X-ray energies used in this study.

The displacement correction factors shown in the above tables vary with the dose stress ranging from maximum value

at the interface to a zero at the equilibrium region. Accordingly the effective measuring point of the TLD shifted toward the radiation stress near to the interface and gradually decreases toward the equilibrium region.

TABLE I
THE MEASURED DOSE BUILD-UP RATIO AT 40 KEV X-RAY EFFECTIVE ENERGY

Interface	Spacer Thickness (microns)	Effective Measuring Point (microns)	Dose Build-up Ratio ± SD
Al - Teflon	0.0	1.46	2.03±0.09
	1.0	2.48	1.70±0.07
	2.0	3.48	1.42±0.09
	4.0	5.49	1.21±0.06
	6.0	7.49	1.04±0.06
Ti-Teflon	0.0	1.39	7.09±0.17
	1.0	2.44	4.50±0.07
	2.0	3.46	3.01±0.07
	3.0	4.46	2.42±0.06
	4.0	5.47	1.42±0.07
	5.0	6.47	1.05±0.05
Cu-Teflon	0.0	1.36	11.56±0.15
	1.0	2.42	6.10±0.05
	2.0	3.45	4.20±0.05
	3.0	4.46	2.65±0.02
	4.0	5.46	1.75±0.03
	6.0	7.47	1.02±0.02
Sn-Teflon	0.0	1.34	18.2±0.42
	1.0	2.41	8.30±0.11
	3.0	4.45	3.92±0.10
	4.0	5.46	1.75±0.03
	6.0	7.47	1.02±0.02

TABLE II
THE MEASURED DOSE BUILD-UP RATION AT 55 KEV X-RAY EFFECTIVE ENERGY

Interface	Spacer Thickness (microns)	Effective Measuring Point (microns)	Dose Build-up ratio± SD
Al - Teflon	0.0	1.47	1.75±0.12
	1.0	2.48	1.59±0.10
	2.0	3.48	1.42±0.04
	3.0	4.49	1.31±0.04
	4.0	5.49	1.09±0.07
	6.0	7.49	1.02±0.07
Ti-Teflon	0.0	1.41	5.54±0.33
	1.0	2.45	3.90±0.23
	2.0	3.46	3.20±0.20
	3.0	4.47	2.38±0.15
	5.0	6.47	1.15±0.15
	6.0	7.48	1.02±0.12
Cu-Teflon	0.0	1.37	9.10±0.19
	1.0	2.43	6.80±0.13
	3.0	4.46	3.30±0.08
	4.0	5.47	2.60±0.09
	5.0	6.47	1.25±0.04
Sn-Teflon	0.0	1.36	14.0±0.36
	1.0	2.43	7.20±0.19
	2.0	3.46	4.10±0.10
	4.0	5.46	3.00±0.06
	6.0	7.47	1.03±0.06

Since the normalized dose build-up ratio, D , varies between 1.0 at the equilibrium region and a high value at the transition region, the formula suggested for the normalized dose build-up ratio is;

$$D = 1 + K \tag{1}$$

where; K is the increase in the normalized dose build-up ratio at the interface region above the equilibrium dose. The K -factor can be fitted very well by an exponential function of the following form.

$$K = \alpha e^{-\beta x} \tag{2}$$

where; α , β are constants for specific energy and material type, and x refer to the distance from the interface. The K -factor, for both X-ray qualities are shown in Figs. 2, 3, 4 and 5.

The constants, α , and β varies linearly with the atomic number as can be seen in Fig. 6 and Fig. 7. We can see that both, α , and β are increases with photon energy.

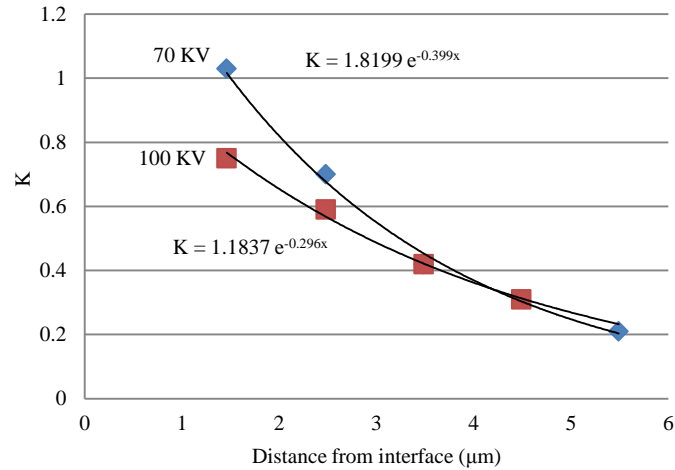


Fig. 2. The K-factor of Al-Teflon interface for 70 KV and 100 KV X-ray potentials.

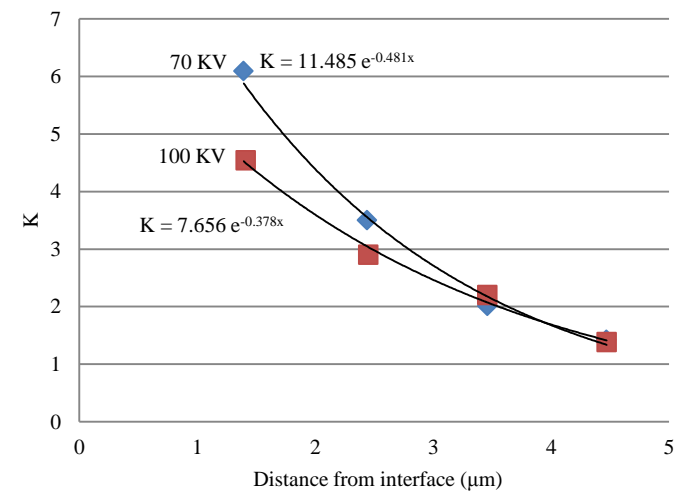


Fig. 3. The K-factor of Ti-Teflon interface for 70 KV and 100 KV X-ray potentials.

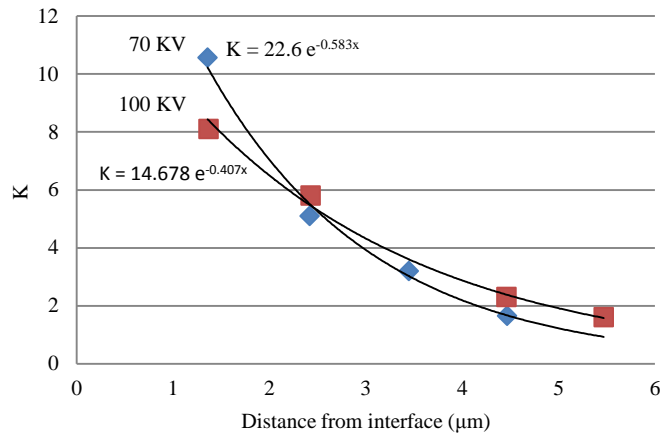


Fig. 4. The K-factor of Cu-Teflon interface for 70 KV and 100 KV X-ray potentials.

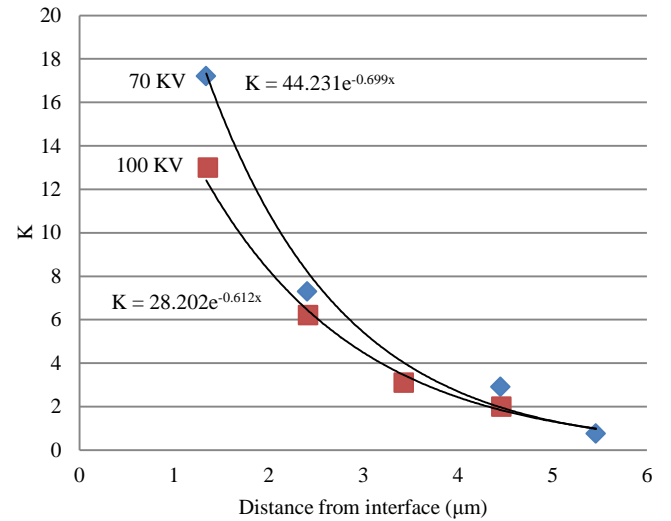


Fig. 5. The K-factor of Sn-Teflon interface for 70 KV and 100 KV X-ray potentials.

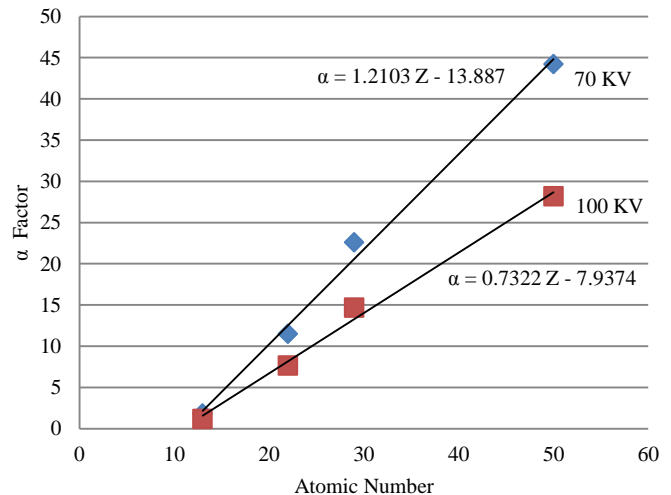


Fig. 6. Variation of α -factor with atomic number.

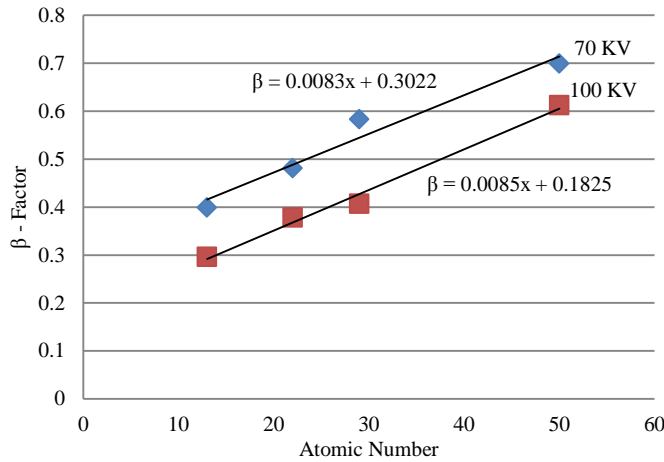


Fig. 7. Variation of β -factor with atomic number.

The formula of (1) is used to estimate the normalized build-up factor for Bone-Teflon interface for both X-ray qualities.

For bone, $Z \approx 14$, in contact with Teflon, $\alpha = 3.0572$, $\beta = 0.3015$, at 100 KV, while $\alpha = 2.3134$, $\beta = 0.4148$ at 70 KV. The calculated dose build-up, D , at the interface is 3.8 times the equilibrium dose 70 KV, while it is about 3.1 at 100 KV, see Fig. 8.

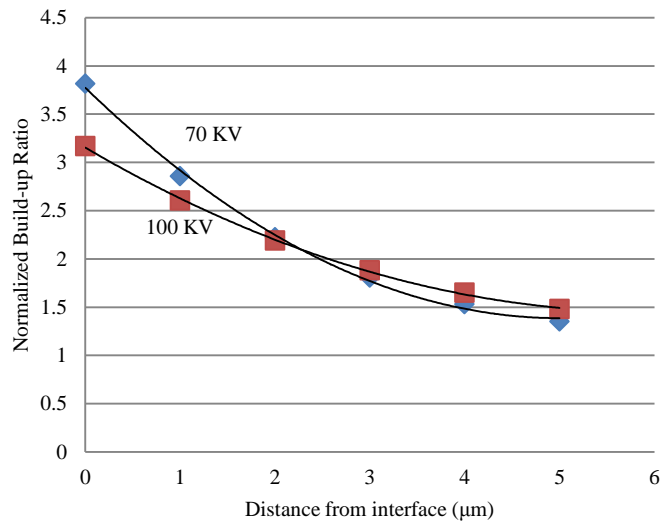


Fig. 8. Estimated normalized dose build-up ratio for Bone-Teflon interface at 70 KV and 100 KV X-ray potentials.

IV. CONCLUSION

Since the experimental data for the dose build-up ratio at low photon energies are very rare due to the technical problems concerning the need of a very thin dosimeter which is unavailable commercially. The ultra-thin TLD developed in our laboratory are excellently used to have 4 to 5 experimental dose readings at the transition region which is only extended for about 10 microns. The present experiment results become valuable source of data at the transition region at low photon energies. The increases in the normalized dose build-up ratio, K -factor, are smoothly fitted by an exponential formula, (2). The formula is used to estimate the normalized dose buildup ratio in Teflon when in contact with Bone. Since the physical absorption and scattering properties of Teflon are close to that for soft tissue, the calculated dose build-up ratio for Bone-Teflon interface indicates that extra care must be considered in determining the dose to Bone Marrow, and soft tissue in contact with Bone at the diagnostic energy range.

REFERENCES

Al-Arif, M.S., 2013a. The Effective Measuring Point of Thermoluminescent Detector at the Build-up Region. *Journal of Natural Sciences and Mathematics, PK*, 52(1), pp.1-7.

Al-Arif, M.S., 2013b. Unity Energy Response Using CaSO₄:DY/Teflon. *ARO, The Scientific Journal of Koya University*, 1(1), pp.14-16. Retrieved from <http://dx.doi.org/10.14500/aro.10026>.

Chandra, P.J., Johnson, D., Vidyasagar, P. B. , Schreiner, L.J., 2010. Dosimetry of interface region near closed air cavities for Co-60, 6 MV and 15 MV photon beams using Monte Carlo simulations. *J Med Phys*, 39(2), pp.73-80.

Das, I.J., Kassae, A., Verhaegen, F. and Moskvina, V.P., 2001. Measurements and Monte Carlo simulations of low-energy photon beams. *Rad Phys and Chemistry*, 61(3), pp. 593-595.

Joshi, C. P., Darko, J., Vidyasagar, P. B., Schreiner, L.J., 2010. Dosimetry of interface region near closed air cavities for Co-60, 6 MV and 15 MV photon beams using Monte Carlo simulations. *J Med Phys*, 35(2), pp.73-80.

Kinhikar, R.A, Tambe, C.M., Patil, K., Mandavkar, M., Deshpande, D.D., Gujjalanavar, R., Yadav, P. and Budrukkar, A, 2014. Estimation of dose enhancement to soft tissue due to backscatter radiation near metal interfaces during head and neck radiotherapy- A phantom dosimetric study with radiochromic film. *J Med Phys*, 39(1), pp.40-3.

Li XA, Yu C. and Holmes, T., 2000. A systematic evaluation of air cavity dose perturbation in megavoltage X-ray beams. *Med Phys*, (27), pp.1011-7.

Nicopoulou-Karayianni, K., Koligliatis, T., Donta-Bakogianni, C., Karayiannis, A. and Litsas, J., 2003. Radiation absorbed doses at compact bone-titanium interfaces in diagnostic radiography: a Monte Carlo approach. *Dentomaxillofac Radiol*, 32(5), pp.327-32.

Shiu, A.S., Hogstrom, K.R., 1991. Dose in Bone and Tissue near Bone-Tissue interface from electron beam. *Int J Radiat Oncol Biol Phys.*, 21(3), pp.695-702.

Lead Removal from Agricultural Soil of Kurdistan Region by Fe₃O₄ Nanoparticles

Karzan A. Omar¹ and Nisar S. Omar²

^{1,2}Department of Chemistry, Faculty of Science and Health, Koya University
University Park, Danielle Mitterrand Boulevard, Koya KOY45, Kurdistan Region of F.R. Iraq

Abstract—Lead toxicity became a major concern worldwide and it is one of the most harmful pollutants in soil and groundwater. Hence, to remove lead from the soil, a high efficient technology with improved materials and system is required. This paper is a study shows removing of lead ions from soil samples, which have been taken from different sites in the Kurdistan Region, and investigated the adsorption of lead ions on high efficient adsorbent Fe₃O₄ nanoparticles. The magnetite nanoparticles of 27nm were synthesized by using a coprecipitation method and characterized by X-ray diffraction (XRD), Fourier Transform Infrared Spectroscopy (FTIR) and scanning electron microscopy (SEM) equipped with energy dispersive X-ray spectroscopy (EDX). The adsorption experiments occurred at pH 8.0 under room temperature (25 °C) and the adsorption capacity was 22.8 mg/g which is 4 times higher than that of coarse particles. The correlation is measured between pH and absorbance, pH and concentration, electrical conductivity and concentration of lead ions in agricultural soil. These relationships indicate that the correlation coefficient values of ($r = -0.68, -0.70$ and $+0.83$) are statistically significant at ($\alpha = 0.05$). The limit of detection (LOD) and limit of quantification (LOQ) were found to be 0.73 mg/L and 2.44 mg/L, respectively.

Index Terms—Adsorption, adsorption capacity, chemical coprecipitation, correlation coefficient, Fe₃O₄ nanoparticles, lead removal, soil.

I. INTRODUCTION

The contamination of soil by lead ions has a serious effect on plants, animals, human being and living organism even at low concentration. It is known to be one of the heavy metals responsible to an environmental pollution by combination with other elements to form different minerals and it is widely used

in industries such as painting, newspaper, television tube, pigments, photographic materials, fuels, batteries.

The manufacturing process of these materials produces wastewaters, usually contain trace amount of lead, which accumulated in soils. The environmental pollution by lead ions causes severe damage to liver, kidney, brain cell, central nervous system in human (Southichak, et al., 2006; Gupta, et al., 1998). The standard concentrations of lead that occur naturally in surface agricultural soils in the range of 7 to 20 ppm with the average 10 parts per million (Holmgren, et al., 1993). Soils with lead levels above this range are primarily the result of lead contamination and according to the World Health Organization (WHO), the US Environmental Protection Agency (USEPA) and Indiana Department of Environmental Management (IDEM) have set standards for lead levels in garden soil or areas where children may come in contact with the soil, the maximum lead level is 400 parts per million (ppm) (Jason, et al., 2007). Due to serious threat mentioned above, research interest has been intensified on development of proper method for removing lead metal from agricultural soil.

The conventional technologies for the removal of heavy metal ions from aqueous solution include chemical precipitation, ion exchange, reverse osmosis, electrochemical treatment and adsorption (Elouear, et al., 2008). Among the different treatments described above, adsorption technology is attractive due to its merits of efficiency, economy and simple operation (Crini, 2005). Lead in soil and groundwater can be effectively removed by using a variety of conventional treatment processes. This paper looks at adsorption of lead on nano-sized magnetite. Fe₃O₄ nanoparticles have been also widely used for magnetic materials, pigments, ferrofluids and catalysts etc., (Cumbal, 2010). Synthesis of nano size iron oxide (Fe₃O₄) nanoparticles can be made by various methods such as; co-precipitation, microemulsion, hydrothermal method, and some novel methods; sonochemical synthesis, arc discharge method, microwave hydrothermal, and one-step hydrothermal process. But in this paper, Fe₃O₄ nanoparticles will synthesis via a Novel Ageing Process because of its simple procedure and pure Fe₃O₄ product (Dong, et al., 1998). The aim of the research is to removing Pb(II) ions from agricultural soil samples, which has been taken from different sites in the Kurdistan Region, by using magnetite

nanoparticles as a high efficient adsorbent through the adsorption process.

II. EXPERIMENT

A. Materials and methods

All the chemicals that used in this experiment were provided by Koya University in Kurdistan Region-Iraq. Ferric chloride ($\text{FeCl}_3 \cdot 6\text{H}_2\text{O}$) and Ferrous Sulfate ($\text{FeSO}_4 \cdot 7\text{H}_2\text{O}$) (Winsford industrial Estate, UK), Urea ($(\text{NH}_2)_2\text{CO}$, Scharlau chemicals, Spain), Lead nitrate ($\text{Pb}(\text{NO}_3)_2$) and Sodium hydroxide NaOH, GAINLAND CHEMICAL, UK), Nitric acid (HNO_3 , Biosolve chimie SARL, France), Hydrochloric acid (HCl), and Acetone (Sd fine-chem limited, Muumbai). All metal solutions were prepared from distilled water.

B. Synthesis of Magnetite Nanoparticles

The chemical reagents used in this preparation of magnetite nanoparticles were Urea: $(\text{NH}_2)_2\text{CO}$, Ferric chloride: $\text{FeCl}_3 \cdot 6\text{H}_2\text{O}$, Sodium hydroxide: NaOH, Ferrous Sulfate: $\text{FeSO}_4 \cdot 7\text{H}_2\text{O}$, and Acetone. A typical approach for this research work is as follow: 5.41 g $\text{FeCl}_3 \cdot 6\text{H}_2\text{O}$ and 3.6 g $(\text{NH}_2)_2\text{CO}$ were dissolved in 200ml distilled water in a container. After that, this solution was placed in a water bath at a constant temperature 90°C . Heating time was 3 hours. The solution turned into a kind of khaki slurry gradually and then it was cooled to room temperature. 1.99 g $\text{FeSO}_4 \cdot 7\text{H}_2\text{O}$ was dissolved in the above mixture with mechanical stirring at a speed of 300 rpm for 30 min. Then, the NaOH solution (2 mol/L) was dropped into the reaction mixture until the $\text{pH} > 10$. Greenish precipitate can be observed at that time. The molar ratio of Fe (III) to Fe (II) in the observed system was nearly 2. When the pH reached greater than 10, the mixture was transferred into an ageing can with a cubage of 500 ml. Additional distilled water was added to make the ageing container full and then it was sealed by a capsule to prevent the air from entering. Finally, the container was aged at room temperature with ageing time such as 5 hr. The black magnetic precipitate was separated by filtration, followed by washing with distilled water of 500 ml and acetone of 100 ml in order. Then, the obtained powders were oven-dried at 50°C for 7 hr.

C. $\text{Pb}(\text{NO}_3)_2$ Stock solution

$\text{Pb}(\text{II})$ stock solution (50 ppm) was prepared by dissolving of lead nitrate $\text{Pb}(\text{NO}_3)_2$ in distilled water.

D. Soil Analyses

This includes;

Standard Soil Tests

To measure pH and electrical conductivity of soil samples was collected from different agricultural sites in Kurdistan Region. The analysis conducted in a soil/water mixture. By taking 2 gm of the agricultural soil of each sample which is mixed with 50ml of distilled water, allowed to be equilibrated for 5 hrs, and then pH and conductivity of the solution would be measured.

Measuring lead concentration in agricultural soil samples

This study was limited to the determination of Pb (II) levels in agricultural soil samples of selected cities located in the Kurdistan Region, namely: Site 1- Koya; Site 2- Darbandixan; Site 3- Bazian; Site 4- Shewashok (2011) and (2014); Site 5- Erbil; Site 6- Shaqlawa; Site 7- Chamchamal; Site 8- Xanaqin; Site 9- Dolly Jafayate; Site 10- Massif; Site 11- Kawer Gosk. Soil samples were collected from eleven sampling sites in each of the study areas. Samples from the selected sampling sites were obtained at a depth 0 to 50 cm from the road. A sample size of 2 gm is generally appropriate of each soil samples were collected from different agricultural sites in Kurdistan Region mixed with 5ml distilled water and 5ml concentrate HNO_3 in a conical flask. After mixing each conical flask which is covered by a watch glass placed concave up in order to reduce gas loss. By refluxing those for 10 min on a hot plate until the vapour condense on the bottom of watch glass and dripped back into the conical flask. Then soil samples were removed on the hot plate added another 5ml concentrated HNO_3 to each flask after cooled down and refluxed for 10 min. Lastly, the soil samples were mixed with 10 ml of distilled water and 5ml concentrate HCl, refluxed for another 15 min. After digesting all soil samples, the filtrate of each solution diluted up to 50 ml in volumetric flask. Then the concentration of the lead would be measured in soil samples by conducting double beam UV-Visible spectroscopy.

E. Lead Removal by Adsorption

The adsorption studies were carried out by mixing 0.05 gm of magnetite nanoparticles with lead solution extracted from soil samples, which was diluted to 50 ml. The pH of the mixture was set to the desired value by using 10M of NaOH. The content of the beaker was stirred uniformly with the help of magnetic stirrer by using magnetic bar for 20 min with 300 rpm at 25°C . The adsorbent was separated from a mixture by filtrations. Then, the amount of Pb (II) absorbed was determined by double beam UV-Visible spectroscopy. As shown by the flow chart in Fig. 1.

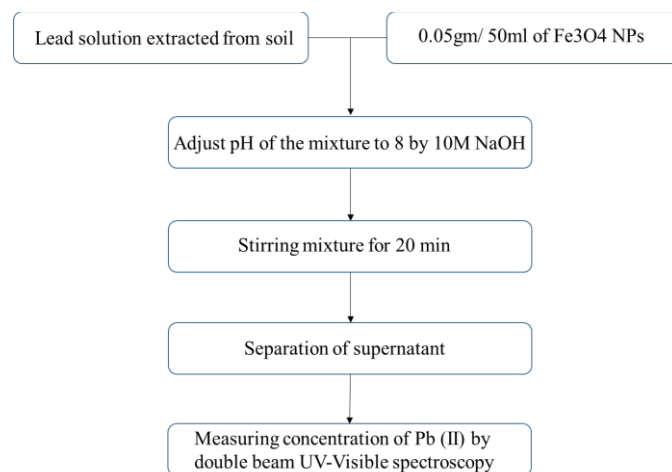


Fig. 1. Steps for removing lead from adsorption process.

III. RESULTS AND DISCUSSION

A. FTIR Analysis of Fe_3O_4 Nanoparticles

Fig. 2. Shows FT-IR spectrum of prepared Fe_3O_4 nanoparticles at room temperature. The spectrum was recorded in the range of $4000-800\text{ cm}^{-1}$. The FT-IR spectrum shows characteristic peaks. The significant absorption peaks observed at 578.12 cm^{-1} is attributed to the Fe-O bond vibration of Fe_3O_4 . The broad absorption peak observed at 3410.07 cm^{-1} reveals the stretching band of H-O-H caused by absorbing water molecules, while the absorption peak at 1618.84 cm^{-1} symbolized the bending band of adsorbed water and absorption peak at 1384.45 cm^{-1} is associated with the hydration water of Fe_3O_4 nanoparticles.

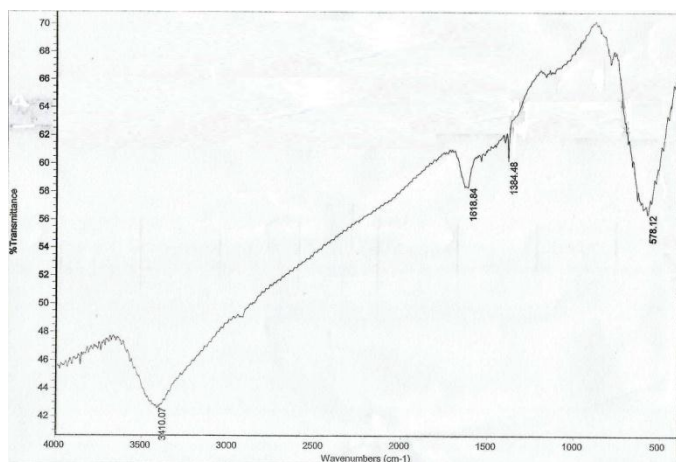


Fig. 2. FTIR spectra of Fe_3O_4 nanoparticles.

B. SEM Analysis of Fe_3O_4 Nanoparticles

The surface morphology of the synthesized magnetite Fe_3O_4 nanoparticles is studied by scanning electron micrograph. As shown in Fig. 3. The SEM images Fe_3O_4 nanoparticles with magnification of 5,000. The instrumental parameters, accelerating voltage, spot size, magnification, and working distances are indicated

SEM image exhibits the agglomeration occurred during the synthesis process. The particles are mostly circular and irregular in shape with a Nano sized range.

C. EDX Analysis of Fe_3O_4 Nanoparticles

The chemical composition of synthesized Fe_3O_4 nanoparticles was studied by using EDX analysis. Table I, shows the ratio of elements which contains weight% and atomic% for all elements and their total ratio equal to 100. Fig. 4. EDX results confirm that the presence of Fe and O in the sample.

TABLE I
CHEMICAL COMPOSITION OF IRON OXIDE NANOPARTICLES

Element	Weight%	Atomic%
O	30.57	59.18
Fe	69.43	40.82
Total	100.0	

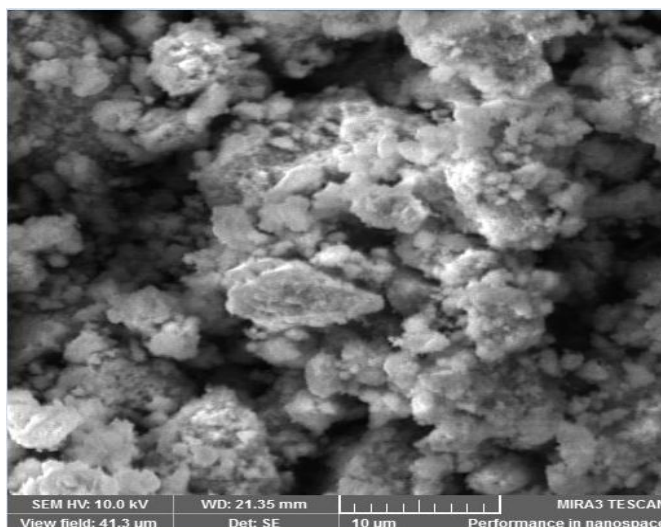


Fig. 3. SEM image of a prepared Fe_3O_4 nanoparticles.

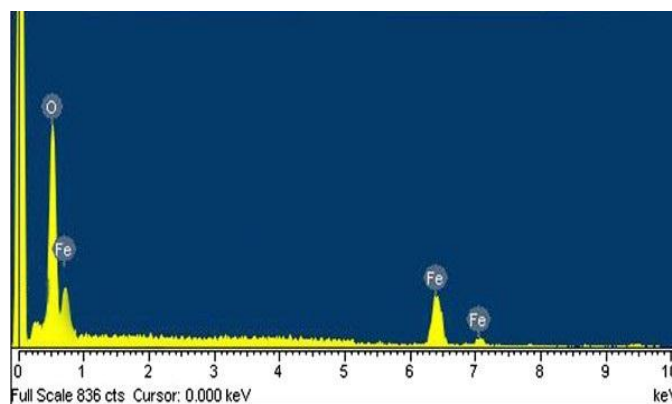


Fig. 4. Energy Dispersive X-ray indicating the chemical composition of prepared Fe_3O_4 nanoparticles.

D. XRD Analysis of Fe_3O_4 Nanoparticles

The ultrafine Fe_3O_4 powders obtained from novel ageing process were characterized by using X-ray diffraction (XRD). XRD was collected by using a Rigaku Mini with Cu $K\alpha$ radiation ($\lambda = 0.1541\text{ nm}$). The diffractograms were recorded in range of $10-80^\circ$. Fig. 5. Shows X-ray diffraction study of magnetite nanoparticles synthesized by chemical Co-precipitation method. From the XRD pattern, it is clear that Fe_3O_4 nanoparticles synthesized purely crystalline in nature.

All the peaks found to be the broadened and indicating the formation of small crystallites. The average particle sizes of synthesized Fe_3O_4 nanoparticles were calculated by using the Debye-Scherrer formula.

$$D = \frac{K\lambda}{\beta \cos\theta} \quad (1)$$

Where 'D' is the mean diameter particle size, 'K' is the shape factor, ' λ ' is the X-ray wavelength (0.1541nm), ' θ ' is the Bragg's angle in radians and ' β ' the full width at half

maximum in radians. The mean diameter particle size is calculated by using the above formula is 27 nm.

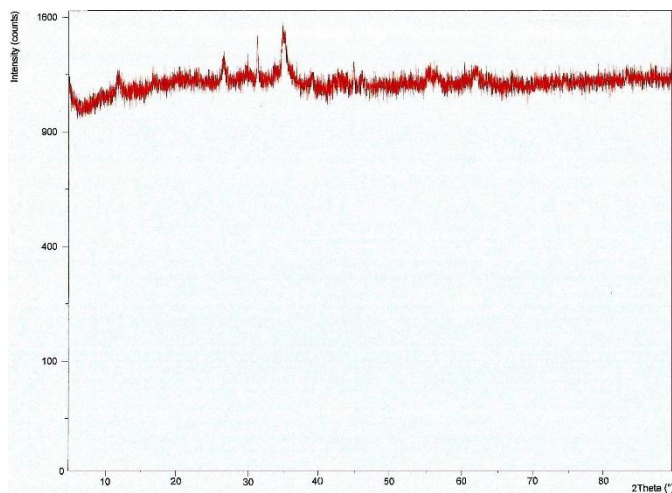


Fig. 5. XRD pattern of prepared Fe₃O₄ nanoparticles

E. Physical analysis of agricultural soil samples

Table II shows the physical properties of the soil. Soil pH was measured in a soil-water 2:50 (w/v) ratio of soil to distilled water by using pH meter according to Davey and Conyers (Davey and Conyers, 1988) while electrical conductivity was determined by the method of Chopro and Kanzar (Chopro and Kanzar, 1988).

TABLE II
PHYSICAL PROPERTIES OF AGRICULTURAL SOIL SAMPLES

Sites	pH	Ec μ s/cm
1	8.14	132
2	8.01	199
3	8.56	121
4	8.06	187
5	8.2	141
6	8.18	134
7	8.25	143
8	7.91	378
9	7.86	380
10	7.83	383
11	7.80	397

The mean pH values of all the soil samples analyzed indicate that the heavy metal-polluted soil samples had low pH values 7.80 – 7.91 relative to the pH values 8.01 – 8.56. It shows that the addition of these metals at these concentrations have lowered the pH of the soil sample. Soil pH is an important soil property, having great effects on solute concentration and adsorption in soil. High soil acidity creates

chemical and biological conditions which may be harmful to plants and soil microorganisms. That the heavy metals from automobile service centers decreased soil pH, thus increasing the soil acidity.

Soil electrical conductivity (EC) also is one of the important soil physical properties, which have a good relationship with the other soil characteristics. Measurement of apparent soil electrical conductivity is the best way of obtaining useful information about soil pollution condition because heavy metals increased soil acidity and electrical conductivity.

F. UV-Visible spectroscopy method

The UV-Visible method for the estimation of lead ions in aqueous solution was validated. Fig. 6 shows the strongest absorption peak of the prepared (50 ppm) Pb(II) stock solution at 305 nm.

The proposed method of determination of lead ions showed molar absorptivity of 1.8×10^4 l/mol/cm and exhibits its maximum absorption at 305 nm. Under the experimental conditions, the calibration graphs of the absorbance versus concentration was found to be linear in the range of 10-50 mg/L for the proposed method. The absorbance (Abs) of the prepared standard solution (10-50 mg/L) was determined at 305 nm. The mean absorbance was found to be 0.2 – 0.9. The absorbance plotted versus concentration as shown in Fig. 7. The linear regression of absorbance on concentration gave equation $y = 0.01997x - 0.0003226$ with a correlation of 0.9997.

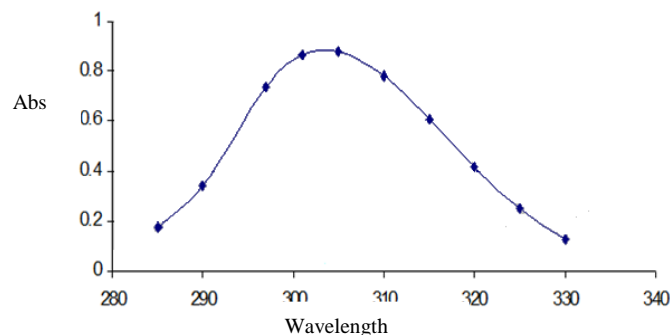


Fig. 6. Determination λ_{max} of Pb(II) ions in stock solution.

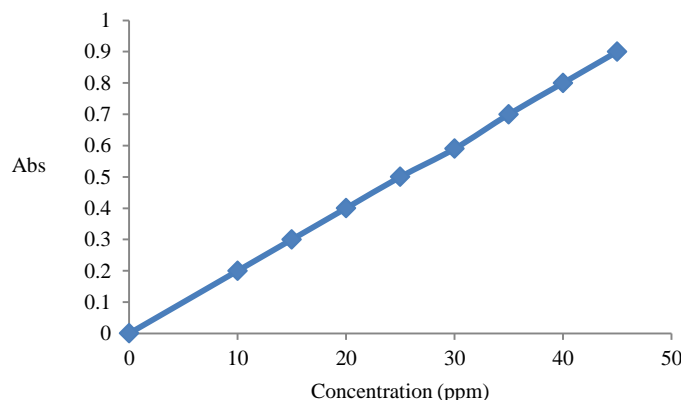


Fig. 7. Calibration curve of Pb(II) in aqueous solution at 305 nm.

G. Limit of Detection and quantification

The limit of detection (LOD) is the lowest amount of analyte in a sample, which can be detected but not necessarily quantified. The limit of quantification (LOQ) is the lowest amount of analyte in a sample. The limit of quantification and the limit of detection were determined based on equations (2) and (3) (Poonan, et al., 2011).

$$\text{LOD} = 3.3\sigma/S \quad (2)$$

$$\text{LOQ} = 10\sigma/S \quad (3)$$

Where, σ is the standard deviation of the intercept of the calibration plot and S is the slope of the calibration curve.

The limit of detection (LOD) and limit of quantification (LOQ) was found to be 0.73 mg/L and 2.44 mg/L respectively as shown in Table III.

TABLE III
VALIDATION PARAMETER FOR STANDARD SOLUTION OF LEAD

Parameter	Values
λ_{max} (nm)	305 nm
Linearity range (mg/L)	10 – 50
Molar absorptivity (l/mol/cm)	1.8×10^4
Intercept (a)	-0.0003225
Slope (b)	0.0199677
Correlation coefficient (r)	0.9997
Regression equation	$y = 0.01997x - 0.0003226$
Limit of detection (LOD)	0.73 mg/L
Limit of quantification (LOQ)	2.44 mg/L

H. UV-Visible Analysis of Pb (II) ions

Study of Pb (II) level in soil samples

The lead concentration in soil samples is collected from different agricultural sites in the Kurdistan Region. It has been measured by double beam UV-Visible spectroscopy as shown in Fig. 8. It can be observed that the lead concentration level in most of sites are in normal range except site 9, 10 and 11; also it shows that the lead concentration in site 4; (2011) was increased compare to (2014), therefore, the preconscious steps should be taken into consideration to prevent increasing the lead level in the Kurdistan Region's agricultural soil because of with the passing time, the lead level will be increases due to industrial sources, their waste products and acid rain which are threaten Kurdish health and their environmental in the future.

Study adsorption of Pb(II) ions in soil samples

Under the optimized conditions, i.e., pH 8.0 and $T = 25^\circ\text{C}$, 0.05 gm of the synthesized Fe_3O_4 nanoparticles with 27nm particle size were used for removing extracted lead ions in agricultural soil samples by stirring it with extracted lead ions from soil samples for 20 min. Then the filtrated was analyzed for remaining Pb(II) concentration in soil samples after the adsorption process as shown in Fig. 9.

The adsorption rate and available capacity of magnetite nanoparticles (adsorbent) are decreased by the diffusion limitation within the particles on a combination of organic

matter which present in agricultural soil and inorganic Fe_3O_4 particle at the Nano-sized level for its high specific area. The observed pH confirmed that the agricultural soil samples are rich with organic matter.

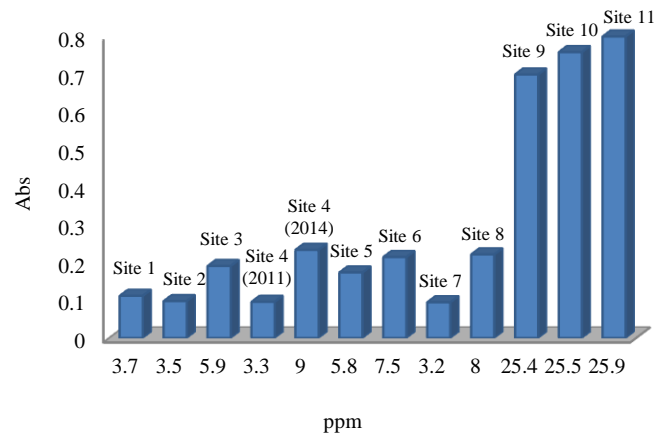


Fig. 8. Lead concentration in different sites of agricultural soil samples.

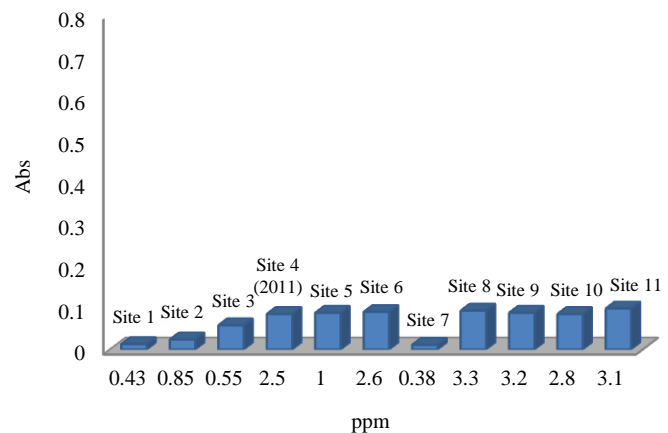


Fig. 9. Lead concentration in agricultural soil samples after adsorption process.

The adsorption rate and available capacity of magnetite nanoparticles (adsorbent) are decreased by the diffusion limitation within the particles on a combination of organic matter which present in agricultural soil and inorganic Fe_3O_4 particle at the Nano-sized level for its high specific area. The observed pH confirmed that the agricultural soil samples are rich with organic matter.

Study of Lead Removal in soil samples

Fig. 10. Shows the percent removal of Pb(II) in soil samples by magnetite nanoparticles adsorbent, and the %Removal of lead was calculated by the following equation:

$$\% \text{Removal of Pb(II)} = \frac{C_{\text{initial}} - C_{\text{final}}}{C_{\text{initial}}} \times 100 \quad (4)$$

Where; $C_{initial}$ is a concentration of Pb(II) ion (mg/L) before adsorption, and C_{final} is a concentration of Pb(II) ion (mg/L) after an adsorption process.

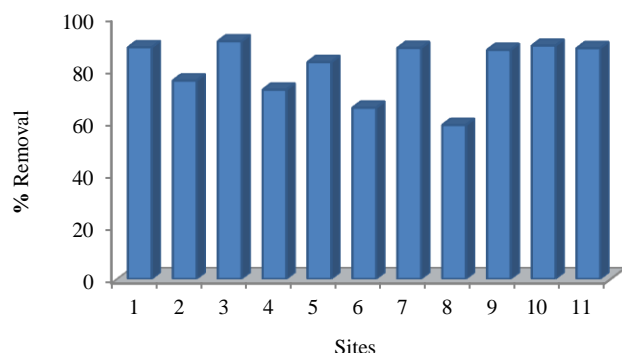


Fig. 10. Lead removal from different sites of agricultural soil in Kurdistan Region.

Study adsorption capacity of adsorbent nanoparticles for removing Pb(II) ions in soil samples

The adsorption experiments were performed in extract lead solution from soil samples at pH 8 and 25°C. The adsorption capacity (Q_e) was calculated by following equation:

$$\text{Adsorption Capacity (} Q_e \text{)} = \frac{(C_o - C_e)V}{W} \quad (5)$$

Where, C_o is the initial concentration of Pb(II) ion (mg/L), C_e is the concentration of Pb(II) ion (mg/L) at equilibrium, V is the volume of Pb(II) ion solution (L) and W is the weight of magnetite nanoparticles used. It was observed the efficiency of Fe_3O_4 nanoparticles as an adsorbent to remove the Pb(II) ions in soil samples was around 22.8 mg/g.

Study effect of pH on adsorption

The charge density of metal oxide surface is a main factor affecting the adsorption of analytes and it varies strongly with pH. Thus, pH is a very important parameter and it plays a major role for the adsorption of target compounds.

The Fe_3O_4 nanoparticles do not exhibit obvious adsorption of lead when the pH value was lower than 8.0. With increasing pH, the adsorption efficiency, increased dramatically and reached maximum when the pH was between 8.0 and 9.0. This is mainly due to the fact that negative charges were favorable for the adsorption of cationic surfactants. When pH value was around Fe_3O_4 nanoparticles isoelectric point (about 7.0) the charge density of Fe_3O_4 nanoparticles surface was very low (Zhao, et al., 2008). When the pH value was above their isoelectric point, the Fe_3O_4 nanoparticles surface became negatively charged which gave rise to the strong electrostatic attraction between the Fe_3O_4 nanoparticles surface and lead ions. But, at pH higher than 9.0, lead can precipitate as hydroxide form. Therefore the pH between 8.0 and 9.0 is favorable for the adsorption lead on adsorbent nanoparticles. Under this condition the pH of 8.0 was selected for this study.

Correlation between lead concentration and physical properties of agricultural soil.

The correlation analysis is one of the most widely statistical methods used in scientific research. In this research correlation coefficient used to determine the relationship between two different variables such as pH and electrical conductivity with absorbance and concentration. Soil pH significantly correlated with absorbance and concentrations of lead in agricultural soil. The negative correlation coefficient of ($r = - 0.68$ and $- 0.70$) is shown in Fig. 11 and Fig. 12. They indicate an inverse relationship between pH and absorbance, pH and concentration of lead in soil samples as pH increases, absorbance and concentration will decrease.

The positive correlation coefficient of ($r = + 0.83$) is observed between electrical conductivity of the soil solutions and the concentration of lead in soil samples as shown in Fig. 13. It indicates a direct relationship between electrical conductivity of soil solutions and the concentration of lead in soil samples. As the concentration of lead in soil samples increases, the electrical conductivity of soil solutions will increase.

The coefficient of determination (r^2) which is calculated for the relationship between pH and absorbance is ($r^2 = 0.46$), in percentage form indicates that only 46% of the total variation of pH could be accounted for by variation of absorbance.

The coefficient of determination which is calculated for relationship between pH and concentration is ($r^2 = 0.49$), in percentage form indicates that only 49% of the total variation of pH could be accounted for by variation of concentration.

The coefficient of determination which is calculated for the relationship between EC and concentration is ($r^2 = 0.68$), in percentage form indicates that only 68% of the total variation of EC could be accounted for by variation of concentration.

The correlation coefficient of ($r = - 0.68$, $- 0.70$ and $+ 0.83$) indicate a statistical significant linear relationship at ($\alpha = 0.05$) which exist between these variables.

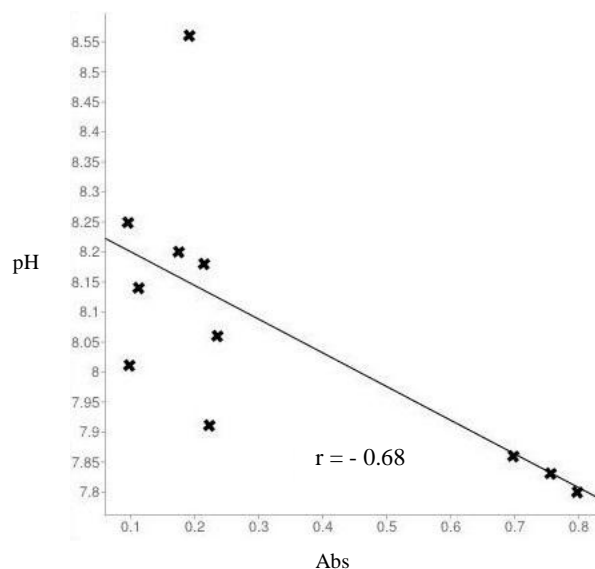


Fig. 11. Correlation between pH and (Abs) Absorbance.

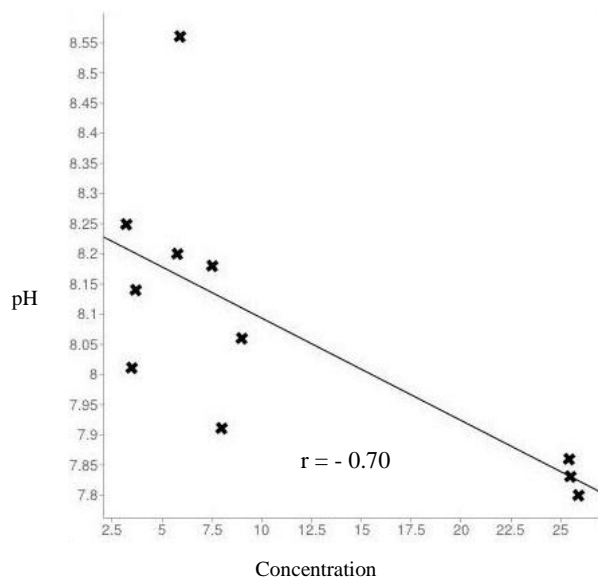


Fig. 12. Correlation between pH and concentration (ppm).

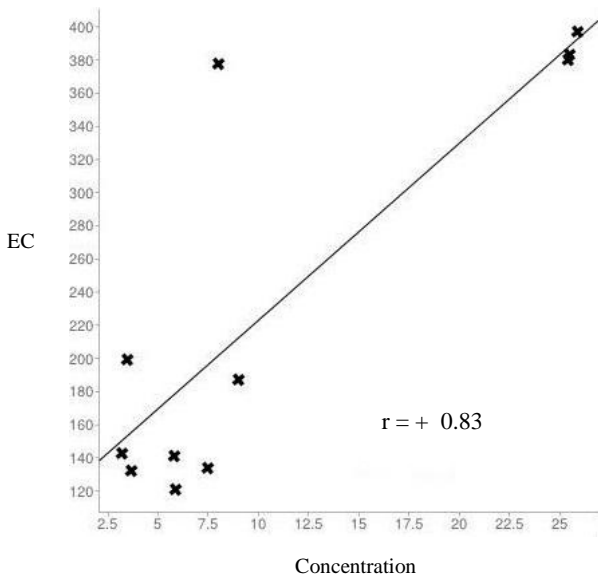


Fig. 13. Correlation between EC and concentration (ppm).

IV. CONCLUSION

Novel Fe_3O_4 nanoparticles have been synthesized successfully through the chemical co-precipitate method. FT-IR, SEM-EDX and XRD characterization techniques confirm the results. UV-Visible spectroscopy method was validated in a term linearity range. The limit of detection (LOD) and limit of quantification (LOQ) were found to be 0.73 mg/L and 2.44 mg/L, respectively. Therefore, it was used for determining the lead concentration before and after adsorption processes.

Fe_3O_4 nanoparticles were applied as an adsorbent for removal of Pb(II) ions from an extracted solution of agricultural soil samples, which was collected from different sites in Kurdistan Region at pH 8 and 25 °C temperature. The Pb(II) ions adsorbate adsorbed on the Nano-adsorbent is

relatively rapid and reaches equilibrium within 20 min stirring. The present results suggest that the adsorption capacity of Fe_3O_4 nanoparticles strongly depends on the surface area of adsorbent, pH and organic matter in agricultural soil.

The adsorption mechanism mainly depends on the electrostatic attraction under the room temperature (25°C) and pH 8. The Fe_3O_4 nanoparticles with the particle size 27 nm can be effectively used to absorb Pb (II) ions in the agricultural soil. The adsorption capacity of Fe_3O_4 nanoparticles reached to 22.8 mg/g, nearly 4 times higher than that of the coarse particles. The percentage removal of toxic Pb(II) ions is, 88.37 mg/L in Site 1, 75.71mg/L in site 2, 90.69 mg/L in site 3, 72.22 mg/L in site 4 (2014), 82.75 mg/L in site 5, 65.33 mg/L in site 6, 88.12 mg/L in site 7, 58.72 mg/L in site 8, 87.40 mg/L in site 9, 89.01 mg/L in site 10, 88.03in mg/L in site 11. Therefore, it is expected that the Fe_3O_4 nanoparticles with the fine range will be used as one of the effective, convenient and low-costing method for removal Pb(II) ions from agricultural soil. The correlation coefficient between pH with absorbance and concentration, showed strong negative linear ship and electrical conductivity with concentration of lead ions in agricultural soil, showed strong positive linear ship which was indicated as a statistical significant which existed between variables.

ACKNOWLEDGMENT

The authors are grateful to Dr. Tara Fuad Tahir, Dr. Shwan Kamal Rashid, Dr. Fahmi Fariq Muhammad and Dr. Fuad Khoshnaw for their support and cooperation.

REFERENCES

- Chopra, G., Kanzar, C., 1988. *Analytical agricultural chemistry*. 2nd edition: Prentice Hall, India, pp.152-160.
- Crini, G.g., 2005. Recent developments in polysaccharide-based materials used as adsorbents in wastewater treatment, *Prog. Polym. Sci.*, 30(1), pp.38–70.
- Cumbal, D., 2010. Preparation of Fe Oxide Nanoparticles for Environmental Applications: Arsenic Removal, *Environ Geochem Health*, 32(4), pp.291-296.
- Dawey, B.G., Conyers, M.K., 1988. Determining the pH of acid soils. *Soil Sci.*, 146(3), pp.141-150.
- Dong, S.B., Kyoug, S.H., Seung, B.C., Sang, H.C., 1998. Synthesis of Ultrafine Fe_3O_4 Powder by Glycothermal Process, *Materials letters*, 37, pp.255-258.
- Elouear, Z., Bouzid, J., Boujelben, N., Feki, M., Jamoussi, F., Montiel, A., 2008. Heavy metal removal from aqueous solutions by activated phosphate rock, *J. Hazard. Mater.*, 156(1), pp.412–420.
- Gupta, V.K., Mohan, D., Sharma, S., 1998. Removal of lead from wastewater using bagasse fly ash-a sugar industry waste material, *Sep. Sci. Technol.*, 33(9), pp. 1331–1343.
- Holmgren, G.G., Meyer, M.W., Chaney, R.L., Daniels, R.B., 1993. Cadmium, lead, copper, and nickel in agricultural soils of the United States of America. *Journal of Environmental Quality*, 22(2), pp.335-348.

Jason, P.K., Brad, D.L., Schwab, A.P., 2007. Protecting Your Family from Lead in the Home —HENV-101-W9. Home & Environment Web site.

Poonam, S.K., Yogesh, V.P., Kishor, B.B., Samina, A.J., Snehal, P.M., 2011. Development and validation of UV spectrophotometric method for the determination of Gliclazide in tablet dosage form. *Der Pharma Chemica*, 3(4), pp.338-343.

Southichak, B., Nakano, K., Nomura, M., Chiba, N., Nishimura, O., 2006. *Phragmites australis*: a novel biosorbent for the removal of heavy metals from aqueous solution. *Water Res.*, 40(12), pp.2295–2302.

Zhao, X., Shi, Y., Wang, T., Cai, Y., Jiang, G., 2008. Preparation of silica-magnetite nanoparticle mixed hemimicelle sorbents for extraction of several typical phenolic compounds from environmental water samples. *J. Chromatogr., A* 1188, pp.140–147.

Non-Destructive Method for Estimating Log Volume for *Melia Azedarach* L. Trees in Erbil-Iraqi Kurdistan Region

Talat M. Amin

College of Agriculture, Salahaddin University
Zanko Street, Kirkuk Road, Erbil, Kurdistan Region of F.R. Iraq

Abstract—The accuracy of four traditional formulas (Smalian, Huber, Bruce and Newton) to calculate log volumes was compared and tested against volumes determined by the water-displacement technique (xylometer). 150 standing trees were measured in a Sami Abd-Alrahman Plantation Park in Erbil governorate on 1 May, 2012. The accuracy of these four procedures was analyzed considering merchantable outside bark volumes of logs of large, mid-and small diameter. The results showed that Newton's formula was superior for all volumes and log lengths considered. Thus, Newton's formula could be used in the majority of circumstances for log lengths of *Melia azedarach* trees. Applying the Newton formula to the tree volumes, DBH and height presented the best fit regression equation which for use in predicting the log volume of *Melia azedarach* trees in Erbil Governorate.

Index Terms— Erbil of Iraq, *melia azedarach*, volume table.

I. INTRODUCTION

Methods of deriving log volume are still important, although weight measurement is being used increasingly for sale of logs. Stem volume is a function of a tree's height, basal area, shape and bark thickness. It is therefore one of the most difficult parameters to measure, because an error in the measurement or assumptions for any one of the above factors will affect the volume estimate. There are different tree volumes: *biological volume*, which is the volume of stem with branches trimmed at the junction with the stem, but usually excluding irregularities not part of the natural growth; *merchantable volume* that excludes some volume within irregularities of the bole shape caused by normal growth in addition to those irregularities not part of natural growth; *gross volume* estimates, which include defective and decayed

wood, and finally *net volume* estimates, which exclude defective and decayed wood (Cris, 2006).

The development of a volume table requires volume equations for the species in question. There are three types of volume equations based on the number of variables and objectives. Each type is formulated by means of regression analysis. These volume equations are: Local volume equation, Regional volume equation and General or Standard volume equation, and we used the third equation type was used in this research. Also for preparation of volume tables there are two methods available to generate volume tables, namely the destructive and the non-destructive method (Adhikari 2005). In the destructive method, 40-50 individuals of a particular species, representing all diameter classes of interest are selected randomly and felled. While the second method, used here, called the Non-destructive method which is similar to the destructive method but the trees are not felled.

Hakki (1999) used Centroid Sampling for testing 21 logs of Ash (*Fraxinus angustifolia* subsp. *oxycarpa*), 38 logs of Spruce (*Picea orientalis* (L.) Link.), and 33 logs of Beech (*Fagus orientalis* Lipsky.). The volume of each log was estimated using Huber's, Smalian's, Newton's, Riecke's and Hosfeld's formulas and Centroid Sampling. These estimates were compared with the "true" volume of each log which was determined by aggregating the volumes of measured short sections (1 m) using Smalian's formula. The mean error of the Centroid estimate of the log volumes was not significant for *Fraxinus angustifolia* subsp. *oxycarpa*, *Picea orientalis* (L.) Link. Or *Fagus orientalis* Lipsky. And was less than those derived from Huber's, Smalian's, Newton-Riecke's, and Hosfeld's formulas. When the three species were combined, the Centroid estimate was clearly more accurate, and its mean error was not significant at 0.05 probability.

Filho, et al. (2000) prepared log volume tables by testing the accuracy of log volume calculation procedures against water displacement techniques (xylometer). Three traditional formulas to calculate log volumes (Smalian, Huber, and Newton) and three recent methods (cubic splines, centroid sampling, and overlapping bolts) were compared and tested against volumes determined by the water-displacement technique (xylometer). Fifty-two felled trees were measured in a *Pinus elliottii* Engelm. Plantation. The accuracy of these six procedures was analyzed considering total and merchantable

ARO, The Scientific Journal of Koya University
Volume II, No (2)2014, Article ID: ARO.10027, 05 pages
DOI: 10.14500/aro.10027
Received 02 September 2013; Accepted 26 October 2014
Regular research paper: Published 23 December 2014
Corresponding author's e-mail: Talat_1952@yahoo.com
Copyright © 2014 Talat M. Amin. This is an open access article distributed under the Creative Commons Attribution License.

outside bark volumes with 1, 2, 4, and 6 m log lengths. The results showed that Huber's formula was superior for all volumes and log lengths considered. Centroid and Newton had a similar performance to Huber but with some higher errors.

Ozcelik, et al. (2006) compared the Centroid, Center of Gravity, Newton, Bruce, Huber, and Smalian formulas for predicting log volumes of three species in Turkey showed the Newton, Center of Gravity, and Centroid methods were clearly superior to the other formulae. The accuracy of all the methods, as indicated by Chi-square accuracy tests, ranged from Newton, Center of Gravity, Centroid, Huber, Bruce to Smalian's formula which performed the poorest.

Amin (2010) estimated merchantable volume and total tree volumes, used the centroid method and depended on it as a dependent variable with DBH and height (pole) as independent variables to make a regression equation connecting these variables for *Quercus agilops* L. trees in Erbil Governorate for total and merchantable volume tables.

The objective of this research is to prepare a *Melia azedarach* log volume table for the first time in Kurdistan region and Iraq, by comparison between more than one methods of estimating tree volumes in order to use it in forestry researches.

II. MATERIAL AND METHOD

Data were collected from Sami Abd-Alrahman Park in Erbil Governorate on 1 May, 2012 to supply the empirical side of this research. The data about the diameters and height of the trees are listed in appendix A.

When using the formulas which are less common, a mid-length log diameter is required. Bruce (1982) derived a formula using only end diameters and length that was popular in some places in forested countries. These formulae are shown below:

Huber: $V = M \cdot L$

Smalian: $V = (B + S/2) L$

Newton: $V = ((B + 4M + S)/6) L$

Bruce: $V = (0.25B + 0.75S) L$

Where: B = cross-sectional area at large end of log; M= cross-sectional area at mid-length of log; S = cross-sectional area at small end of log; L = log length (m).

From the application of the above formulas the volume of each tree in the sample was found, depending on the data collected. After calculating the cross-sectional areas of large, mid-and small ends of log length, the volumes of the trees were as follow in Table I.

TABLE I

VOLUMES OF SAMPLE TREE ESTIMATING BY USING VOLUME FORMULA

No.	Plot	Huber	Smalian	Newton	Bruce
1	1	1899.7	1397.3	1732.2	769.3
2	1	1275.2	918.5	1156.3	522.8
3	1	1020.9	805.8	949.2	466.5

4		2077.1	1441.3	1865.2	805.4
5		750.6	630.9	710.7	375.5
6		314	386.6	338.2	249.8
7		188.4	301.7	226.1	203.8
8		356.2	341.5	351.3	223.7
9		1020.8	880.1	973.9	503.6
10		500.1	436.5	478.8	264.2
11		17.6	98.1	44.4	84.3
12		56.5	78.5	63.8	67.5
13		395.6	401.1	397.4	250.1
14		339.1	325.2	334.5	205.1
15		480.4	542.1	500.9	331.1
16		255.1	352.3	287.5	222.1
17		206.6	393.2	268.8	242.5
18		113.1	181	135.7	122.3
19		1557.8	1257.5	1457.7	692.3
20		2279.6	1931.1	2163.4	1050.3
21		1884	1616.1	1794.7	892.8
22		2918.6	2152.2	2663.1	1153.8
23		2077.1	1801.5	1985.2	985.5
24		1004.	1020.5	1010	580.9
25		954.5	776	895	455.1
26		1191	1117.3	1166.5	632.9
27		1644.3	1140.9	1476.6	637.6
28		3114.5	2413.9	2880.9	1312.9
29		356.2	362.4	358.2	234.2
30		1134.3	1042.2	1103.6	591.7
31		907.4	782.2	865.7	447.6
32		1191	1311	1231	729.7
33		794.8	805.8	798.4	466.5
34		596.9	651.8	615.2	389.5
35		803.8	732.5	780	422.7
36		846.2	962.9	885.1	559.1
37		803.8	716.3	774.6	414.6
38		1899.7	1609.2	1802.8	875.2
39	2	729.6	1122.5	860.6	638.9
40	2	1004.8	1086.3	1031.9	613.8
41	2	846.2	1321.2	1004.5	738.2
42		1972.5	1635.1	1860	884.6
43		427.4	487.9	447.5	307.5
44		2279.6	2275.5	2278.2	1222.5
45		618.2	655.3	630.5	377.1
46		461.5	490.1	471	287.4
47		907.4	684.5	833.1	398.8
48		452.2	510.3	471.5	311.6
49		356.1	529.9	414.1	317.9
50		883.1	855.7	873.9	498.5
51		2512	2235.7	2419.8	1230.9
52		1059.8	725.9	948.4	447.7
53		576.9	490.9	548.3	298.5
54		1474.6	1500.7	1483.3	842.2
55		923.5	1074.5	973.5	622
56		1406.7	1489.8	1434.4	843.8
57		1558.6	1269.8	1462.3	712.6
58		1256	1330.2	1280.7	753.4
59		1247.8	1098.9	1198.1	627.1
60		1558.6	1426.9	1514.7	791.1
61		3114.5	2173.2	2800.7	1192.6
62		2267.1	1921.7	2151.9	1073.9
63		1361.2	1413.1	1378.5	791.3
64		3046.7	2951.9	3015.2	1719.7
65		1038.6	1236.1	1104.4	713.4
66		1306.2	1561.3	1391.2	872.5
67		1000.1	1112.3	1037.5	648
68		546.1	895.9	662.8	529.2
69		510.3	829.1	616.5	506.4
70		522.4	941.2	662	548.3
71		846.2	1029.7	907.3	592.6
72		971.4	1219.6	1054.2	687.5
73		1727	1537	1663.7	846.2
74		2250.2	1951.7	2150.7	1067.7
75		621.7	984.9	742.8	570.1
76		1474.6	1654.6	1534.6	919.2
77	3	508.7	668	561.8	397.6

78	3	2279.6	1801.6	2120.3	985.6
79	3	1558.6	1122.6	1413.2	638.9
80		1004.8	1020.5	1010	580.9
81		226.1	362	271.4	244.6
82		2077.1	1676.8	1943.7	923.2
83		2163.7	1621.56	1982.9	899
84		1361.2	1330.6	1350.9	750.1
85		508.7	604.4	540.6	365.8
86		2423.3	2489.9	2445.5	1343.8
87		1474.6	1271.2	1406.8	727.4
88		2119.5	1621.4	1953.4	906
89		884.7	1052.9	940.8	607.7
90		1356.5	1320	1344.3	755.4
91		1644.7	1741.5	1677	973.2
92		596.9	842.5	678.8	484.8
93		3581.9	2724.2	3296	1457.5
94		474.9	706.5	552.1	423.9
95		1884	1801.6	1856.5	985.6
96		1531.3	1818.1	1626.9	1004.4
97		2336.7	2323.5	2332.3	1257.1
98		1304.4	1381.2	1330	771
99		1716.8	1886.4	1773.3	1038.6
100		1912.8	1818.1	1881.3	1004.4
101		2564.6	1621.4	2250.2	906.1
102		3189	2349.8	2909.3	1266.8
103		1962.5	1811.02	1912.007	993.8223
104		2564.6	2026.7	2385.3	1108.7
105		1077.6	1140.9	1098.7	637.6
106		2387.7	1788	2187.852	975.2
107		1335.3	1212.1	1294.2	680.2
108		1361.2	1224.6	1315.7	697.1
109		2595.4	2259.4	2483.4	1218
110		3316.6	2759.8	3131	1468.2
111		2599.9	2690.2	2630	1426.3
112		2119.5	1621.4	1953.4	906
113		2699.2	2387.9	2595.4	1285.8
114		2423.3	1816.1	2220.9	1006.9
115		2250.2	2504.2	2334.8	1343.9
116	4	923.2	1074.5	973.5	622
117	4	1361.2	1224.6	1315.7	697.1
118	4	904.3	770.1	859.6	448.6
119		497.4	453.7	482.9	279.8
120		692.4	918.5	767.7	522.8
121		1361.2	1330.6	1350.9	750.1
122		1570	1397.3	1512.4	769.3
123		907.5	1037.8	950.9	575.4
124		284.9	382.7	317.5	233.7
125		1921.7	1876.6	1906.7	998.3
126		84.8	211.9	127.2	148.4
127		883.1	936.1	900.8	538.7
128		1134.3	1108.8	1125.8	625
129		403.6	542.1	449.8	331.1
130		395.6	494.6	428.6	296.7
131		538.5	908	661.7	503.4
132		971.4	857	933.3	506.2
133		1148	1383.4	1226.5	783.5
134		1570	1297.2	1479	719.2
135		1361.2	1330.6	1350.9	750.1
136		2491.6	1931.1	2304.8	1050.3
137		1134.3	1201.1	1156.6	671.2
138		2163.7	2407.9	2245.1	1292.3
139		1192.2	1263.7	1216	727.2
140		1589.6	1501.3	1560.2	838.9
141		1462.5	1491.7	1472.2	827.1
142		1805.5	1606.9	1739.3	884.7
143		884.7	895.9	888.5	529.2
144		653.9	761	689.6	440.5
145		356.1	641.7	451.4	373.8
146		1471.3	1344.6	1429	732.4
147		1306.2	1686.4	1432.9	935
148		2089.7	2020.6	2066.6	1088
149		593.5	898.4	695.1	523.4
150		904.3	842.5	883.7	484.8

The field work also included felling two trees (there was no ability or permission to fall more trees) to find their volumes using water displacement by the xylometer method. The accuracy of four traditional formulas for calculating log volumes was compared and tested against the volumes determined by the water-displacement technique (xylometer). The results showed that the Newton formula was superior for all tree volumes and had the best results. We replied on the tree volumes estimated by this formula in preparing the volume Table for *Melia azedarach* trees. These results are compatible with the results of Filho, et al. (2000) and Ozcelik, et al. (2006).

III. RESULTS AND DISCUSSION

Diameters were measured at different heights by climbing the trees. In the Equation Method, while the basic data essentially remain the same as in the graphical method, the relationships between volume as a dependent variable and DBH, hight and form, etc as independent variables are given mathematical expressions by a regression equation. Various workers have developed various equations or models, some of them are: Meyor modified, Austrian, Combined variable, Constant Form Factor, Logarithmic, and others (Chaturvedy and Khanna 2000). The results from using three of these equations and testing them are presented in Table II.

TABLE II
STANDARD VOLUME REGRESSION EQUATIONS USING LOG TREE VOLUME WITH THEIR MEASURES OF PRECISION TEST, FROM DATA OF ALL SAMPLE PLOT TREES FOR *MELIA AZEDARACH* IN ERBIL GOVERNORATE

Regression Equations	b_0	b_1	b_2	$R^2(\text{adj})\%$	S.E
$V = b_0 + b_1D + b_2H$	-481.665	-0.00538789	329.358	48.6184	522.585
$V = b_0 + b_1DH$	-458.44	15.67	.	89.6368	235.484
$V = b_0 + b_1 \log D + b_2 \log H$	-5557.21	4044.61	2266.86	77.7774	343.677

$V =$ Tree volume
 $D =$ Tree diameter
 $H =$ Tree height
 $b_i =$ Parameters

According to the value of the adjusted coefficient of determination in Table II we can see that the second equation has the best fit regression equation (the highest R^2 value equals to 0.89 and the lowest standard error value equals to 235.48, in comparison with other models or equations). This second equation can be used for preparing a log volume table for *Melia azedarach* trees in Erbil Governorate using different values for diameter at breast height and different values for trees height.

IV. RECOMMENDATIONS

From the results of this research we recommend the use of the regression equation for preparing a volume table for *Melia azedarach* trees by those interested in this field because it is easy to assess the volume of standing trees and easy to use, whilst the calculation is time, money and manpower consuming, and needs extra instruments, whereas, a volume table does not. A volume table is more convenient, easy to apply in the field, and measurements and calculation can be done simultaneously.

APPENDIX A

DATA COLLECTION FOR MELIA ASEDARACH TREES IN ERBIL GOVERNORATE

No	Loc.	Plot	do 30 cm	dbh	D at mid	H	hi d6cm
1			26	25	22	8	5
2			22	20	19	7.50	4.50
3			20.50	18.50	17	8.50	4.50
4			24	23	21	9	6
5			18.50	17.50	15	7.75	4.25
6			14.50	12.50	10	7.25	4
7			13	11.50	8	6.75	3.75
8			14	12	11	6.25	3.75
9			21.50	19.50	17	8	4.50
10			17.50	16.50	14	6.75	3.25
11			8	6.50	3	5.50	2.50
12			8	7	6	4.75	2
13			16	14	12	6.25	3.50
14	Erbil	1	15.50	14	12	6	3
15			17	15	12	6.50	4.25
16			15.50	13.50	10	5.75	3.25
17			16.50	13.50	9	6.25	3.25
18			13	11	8	4	2.25
19			26	25	21	8	4.50
20			28	27	22	10	6
21			25.50	24.50	20	9.50	6
22			31	30	26	11	5.50
23			27	24.50	21	9.50	6
24			22	19.50	16	8.50	5
25			19.50	18.50	16	7	4.75
26			22.50	20	17	9.25	5.25
27			24	23.50	21	10	4.75
28			28	25.75	23	10	7.50
29			14.50	13.75	11	8.25	3.75
30			22.25	21.50	17	9	5
31			21.50	20	17	8.25	4

No	Loc.	Plot	do 30 cm	dbh	D at mid	H	hi d6cm
32			24.50	21.50	17	8.50	5.25
33			20.50	18.50	15	8.50	4.50
34			18.25	15	13	7.75	4.50
35			20.75	19.25	16	8	4
36			20.25	17.25	14	9.50	5.50
37			20.50	19.25	16	8	4
38			28	26	22	8.75	5
39			22	18	13	9	5.50
40			22.75	19	16	9.50	5
41			24	19.50	14	9.50	5.50
42			29	27.25	23	9.25	4.75
43			15.50	14	11	8	4.50
44		2	30.50	26.25	22	9	6
45			21	18	15	7	3.50
46			19.50	18	14	6.50	3
47			20	19	17	8	4
48			17	15.50	12	8	4
49			18	16	11	8	3.75
50			20	18	15	8.50	5
51			26	23	20	11	8
52			16.50	16	15	10	6
53			17.25	16.50	14	8	3.75
54			23.50	20	17	12	6.50
55			20.50	16	14	10.50	6
56			22.50	18.75	16	11	7
57			23.50	21	19	9.50	5.50
58			22.50	18	16	11.25	6.25
59			21.75	18.50	17	10.75	5.50
60	Erbil		25	21	19	12	5.50
61			26.50	25.50	23	12.50	7.50
62			24	21.75	19	12	8
63			23.75	18	17	12	6
64			20	18	15	11.50	17.25
65			20.75	17.75	14	11	6.75
66			24	20	16	11	6.50
67			20	19	14	11	6.50
68			19	18	11	10.25	5.75
69			17	15.50	10	10	6.50
70			20	16.50	11	9.50	5.5
71			21	19.50	14	10	5.5
72			23	19	15	10.50	5.5
73			26	24.50	20	10.50	5.50
74		3	27	24.	21	10.50	6.50
75			20.50	19	12	10	5.50
76			24.75	22	17	10.50	6.50
77			18.50	16	12	9.50	4.50
78			27	26.50	22	10.50	6
79			22	21	19	10.50	5.5
80			22	19.50	16	10.50	5
81			13	11.50	8	9.50	4.50
82			26	24	21	12	6
83			25	23	21	11	6.25
84			23	21	17	10.50	6
85			17.50	15.50	12	9.50	4.50
86			29.50	26.50	21	11.75	7
87			21.50	20	17	10.50	6.50
88			24	22	20	11.25	6.75
89			20.75	18	14	10.25	5.75
90			21.50	20	16	10.50	6.75

No	Loc.	Plot	do 3'0 cm	dbh	D at mid	H	hi d6cm
91			24	21	17	11.25	7.25
92			21	17	13	10.50	4.50
93			31.50	30	26	10.75	6.75
94			18	16	11	9.75	5
95			27	23	20	10.75	6
96			25.50	20.50	17	11.75	6.75
97			29	25	21	10.75	6.75
98			24	21	17	10.75	5.75
99			26	22	18	11.50	6.75
100			25.50	23	19	11.25	6.75
101			24	24	22	10.75	6.75
102			29.75	27.75	25	11.25	6.50
103			26.50	23	20	10.50	6.25
104			27	26.50	22	10	6.75
105			24	22	17	9.50	4.75
106			27.50	26	23	10.50	5.75
107			23.50	21	18	10.75	5.25
108			22	20	17	11	6
109			29.75	27.50	23	11.75	6.25
110			33	29	26	10.75	6.25
111			34	28.50	24	11.25	5.75
112			24	23	20	11.50	6.75
113			30	27	23	10.75	6.50
114			25	24	21	10.50	7
115			30.75	25.75	21	11.75	6.50
116			20.50	19	14	9.50	6
117			22	20	17	9.25	6
118			20	19	16	9.75	4.50
119			16.50	15.5	13	8.75	3.75
120			22	18	14	8.50	4.50
121			23	21	17	9.50	6
122			26	25	20	9.50	5
123			25	22	17	8	4
124	Erbil	4	17	14	11	8	3
125			33	29	24	8.50	4.25
126			12	10	6	6.50	3
127			21	19	15	8.50	5
128			23	21	17	8.75	5
129			17	16	11	7.75	4.25
130			18	15.50	12	7	3.50
131			25	18	14	8	3.50
132			19	18	15	9.25	5.50
133			22.50	18	15	10	6.5
134			25	24	20	9.75	5
135			23	21.75	17	9.50	6
136			28	27	23	10	6
137			24	20.50	17	10	5
138			30.75	25.50	21	10.50	6.25
139			21	19	15	10.75	6.75
140			24	23	18	9.25	6.25
141			25	21	18	10	5.75
142			26	23	20	10	5.75
143			19	18	14	10.75	5.75
144			20.50	19	14	8.75	4.25
145			20	18	11	7.75	3.75
146			27.75	26	21	8.75	4.25
147			25	20	16	10.25	6.50
148			30	27	22	10.75	5.50
149			20	18.50	12	8.75	5.25
150			21	20	16	8.50	4.50

REFERENCES

- Adhikari, M., 2005. *A Non-destructive Approach for Quantitative Assessment of Tree Resources outside the Forest*, Ph.D., International institute for GEO-information, Netherlands.
- Amin, T., 2010. *Study on Tree Biometry Tables and Relationships for Quercus aegilops L. Growing Naturally in Erbil*, M.Sc. University of Sallahaddin, Iraq.
- Bruce, D., 1982. Butt log volume estimators. *Forest Sci.* 28(3), pp.489-503.
- Chaturvedy, A. and Khanna, L., 2000. *Forest Mensuration and Biometrics*. 3rd ed. Khanna Bandhu, Dehradun, India.
- Cris, B., 2006. *Forest Measurement and Modeling*. Australian National University.
- Filho, A., Machado, S. and Carneiro, M., 2000. Testing accuracy of log volume calculation procedures against water displacement techniques (xylometer). *Canadian Journal of Forest Research*, 30(6), pp.990-997.
- Hakki Y., 1999. Comparison of the Centroid Method and Four Standard Formulas for Estimating Log Volumes. *Tr. J. of Agriculture and Forestry*, 23, pp.597-602.
- Ozcelik, R., Wiant, H. and Brooks, J., 2006. Estimating log volumes of three tree species in Turkey by six formulae. *Forest Products Journal*, 56(11/12), pp.84-86.

General Information

Aro's Mission: Aro seeks to publish those papers that are most influential in their fields or across fields and that will significantly advance scientific understanding. Selected papers should present novel and broadly important data, syntheses, or concepts. They should merit the recognition by the scientific community and general public provided by publication in Aro, beyond that provided by specialty journals.

We welcome submissions from all fields of natural science and technology, and from any source. We are committed to the prompt evaluation and publication of submitted papers. Aro is published biannually; selected papers are published online ahead of print.

Submission

Manuscripts should be submitted by the correspondent authors of the manuscript via the on-line submission page (<http://aro.koyauniversity.org./authors/submit-online>). Regardless of the source of the word-processing tool, only electronic Word (.doc, .docx, .rtf) files can be submitted on-line. There is no page limit. Only online submissions are accepted to facilitate rapid publication and minimize administrative costs. Submissions by any other one but the authors will not be accepted. The submitting author takes responsibility for the paper during submission and peer review. If for some technical reason submission through the email is not possible, the author can contact aro.journal@koyauniversity.org for support. Before submitting please check ARO's guide to authors thoroughly to avoid any delay in the review and publication process.

Authors are explicitly responsible for the language of their texts. Paper should be submitted in a well written in an understandable English. Authors should not expect the editor or editorial board to rewrite their paper. Prior to submission, authors should have their paper proofread by a possible academic native speaker of English.

- Submit the Article with contact Information
- File Name should be your article title
- Don't submit your article in multiple journal, we are taking only minimum time for review process. please don't waste our time
- Once the paper is accepted, it can't be withdrawn
- Please follow publication ethics and regulation
- Avoid plagiarism and copied material
- Strictly Follow Aro's Template

Terms of Submission

Papers must be submitted on the understanding that they have not been published elsewhere and are not currently under consideration by another journal or any other publisher. Aro accepts original articles with novel impacts only. Post conference papers are not accepted "as is", however, regular papers on the same topic but with a different title can be submitted. The new paper should contain significant improvements in terms of extended content, analysis, comparisons with popular methods, results, figures, comments, etc. Please do not forget that the publication of the same or similar material in Aro constitutes the grounds for filing of an (auto) plagiarism case.

The submitting author is responsible for ensuring that the article's publication has been approved by all the other co-authors. It is also the authors' responsibility to ensure that the articles emanating from a particular institution are submitted with the approval of the necessary institution. Only an acknowledgement from the editorial office officially establishes the date of receipt. Further correspondence and proofs will be sent to the author(s) before publication unless otherwise indicated. It is a condition of submission of a paper that the authors permit editing of the

paper for readability. All enquiries concerning the publication of accepted papers should be addressed to aro.journal@koyauniversity.org.

Peer Review

All manuscripts are subject to peer review and are expected to meet standards of academic excellence. Submissions will be considered by an editor and “if not rejected right away” by peer-reviewers, whose identities will remain anonymous to the authors.

Guide to Author

We welcome submissions from all fields of science and from any source. We are committed to the prompt evaluation and publication of submitted papers. Selected papers are published online ahead of print. Authors are encouraged to read the instructions below before submitting their manuscripts. This section arranged into an overview speedy guidelines below and more detailed at the bottom section of this page

Manuscript Preparation

Submitting your manuscript will be in two stages namely before final acceptance and after.

Stage one:

At the first stage manuscript needs to be prepared electronically and submitted online via the online submission page in a Word (.doc, .docx, .rtf) format of one column double-spaced page, Times New Roman font type, and 12 p font size. A pdf version of the submitted manuscript should be submitted too. All authors' names, affiliations, e-mail addresses, and mobile phone numbers should be typed on a cover page, indicating the correspondent author.

Stage two:

- File type: MS-Word version 2003 or later.
- Format: The preferred format of the manuscript two-column template with figures and captions included in the text. This template can be downloaded via the following link. Please follow instructions given in the template; <http://aro.koyauniversity.org/authors/guide-for-author>
- Text: All text is in Times New Roman font. The main text is 10-point, abstract is 9-point font and tables, references and captions are 8-point font.
- Figures: Figures should be easily viewed on a computer screen.

Units of Measurement

Units of measurement should be presented simply and concisely using System International (SI) units.

Title and Authorship Information

The following information should be included

- Paper title
- Full author names
- Affiliation
- Email addresses

Abstract

The manuscript should contain an abstract. The abstract should be self-contained and citation-free and should not exceed 200 words.

Introduction

This section should be succinct, with no subheadings.

Materials and Methods

This part should contain sufficient detail so that all procedures can be repeated. It can be divided into subsections if several methods are described.

Results and Discussion

This section may each be divided by subheadings or may be combined.

Conclusions

This should clearly explain the main conclusions of the work highlighting its importance and relevance.

Acknowledgements

All acknowledgements (if any) should be included at the very end of the paper before the references and may include supporting grants, presentations, and so forth.

References

References must be included in the manuscript and authors are responsible for the accuracy of references. Manuscripts without them will be returned. ARO is following Harvard System of Referencing. (Learn how to import and use Harvard Styling in your Microsoft Office by following this link:

<http://bibword.codeplex.com/releases/view/15852>)

Preparation of Figures

Upon submission of an article, authors are supposed to include all figures and tables in the PDF file of the manuscript. Figures and tables should be embedded in the manuscript. Figures should be supplied in either vector art formats (Illustrator, EPS, WMF, FreeHand, CorelDraw, PowerPoint, Excel, etc.) or bitmap formats (Photoshop, TIFF, GIF, JPEG, etc.). Bitmap images should be of 300 dpi resolution at least unless the resolution is intentionally set to a lower level for scientific reasons. If a bitmap image has labels, the image and labels should be embedded in separate layers.

Preparation of Tables

Tables should be cited consecutively in the text. Every table must have a descriptive title and if numerical measurements are given, the units should be included in the column heading. Vertical rules should not be used.

Copyright

Open Access authors retain the copyrights of their papers, and all open access articles are distributed under the terms of the Creative Commons Attribution License, which permits unrestricted use, distribution and reproduction in any medium, provided that the original work is properly cited.

The use of general descriptive names, trade names, trademarks, and so forth in this publication, even if not specifically identified, does not imply that these names are not protected by the relevant laws and regulations.

While the advice and information in this journal are believed to be true and accurate on the date of its going to press, neither the authors, the editors, nor the publisher can accept any legal responsibility for any errors or omissions that may be made. The publisher makes no warranty, express or implied, with respect to the material contained herein.

ARO Reviewer/Associate Editor Application Form

ARO is a scientific journal of Koya University (p-ISSN: 2410-9355, e-ISSN: 2307-549X) which aims to offer a novel contribution to the study of Science. The purpose of ARO is twofold: first, it will aim to become an ongoing forum for debate and discussion across the sciences and Engineering. We hope to advance our problem solving capacity and deepen our knowledge regarding a comprehensive range of collective actions. Second, ARO accepts the challenges brought about by multidisciplinary scientific areas and aspires to expand the community of academics who are able to learn from and help to produce advances in a variety of different disciplines.

The Journal is seeking reviewers who can provide constructive analysis of papers thus enhancing overall reputation of the Journal. If any expert is interested in participating the review process, we highly encourage you to sign up as a reviewer for our Journal and help us improve our presence in domain of your expertise. Appropriate selection of reviewers who have expertise and interest in the domain relevant to each manuscript are essential elements that ensure a timely, productive peer review process. We require proficiency in English.

How to apply

To apply for becoming a reviewer or a member of the Editorial Board of ARO, please submit the application form by following the link:

<http://aro.koyauniversity.org/about/application-form>.

Both Associate Editor and Reviewers should specify their areas of research and expertise. Applicants must have a doctorate (or an equivalent degree), and if Master degree they need to have significant publishing experience. Please note that

- You will need to write you full official name.
- Please provide an email which reflects your official name, such as nameOne.NameTwo@... , or your institute's official email.
- All data need to be written in English.

Note: For more information, kindly visit the following websites:

1. Aro.koyauniversity.org.
2. <http://libweb.anglia.ac.uk/referencing/harvard.htm>.
3. <http://bibword.codeplex.com/releases/view/15852>.

Koya University is located in the city of Koya (Koysinjaq), which is one hour drive to the East of the Kurdistan Region capital Erbil (Erbil, Hewlér) in North Iraq. It is on the foothills of beautiful high mountain. Its campus has been carefully laid out to embrace the beautiful mountainous nature. The Koya University was established in 2003 and has developed noticeably. In 2010, Koya University was restructured from colleges to faculty systems to enhance the interactions between similar academic fields. Today the University has 4 faculties - Engineering, Science and Health, Humanities and Social Sciences and Education, and a school of Medicine- which together compound 25 departments in different fields, such as Petroleum Engineering, Geotechnical Engineering, Clinical Psychology, Social Science and Medical Microbiology, as well as Sport Education.

Aro is a scientific journal published by the Koya University. Aro is a journal of original scientific research, global news, and commentary. The Aro Scientific Journal is a peer-reviewed, open access journal that publishes original research articles as well as review articles in all areas of Natural Science and Technology.



ARO the Scientific Journal Office
Koya University Park
Danielle Mitterrand Boulevard
Koya KOY45
Kurdistan Region - F.R. Iraq